

BULLETIN OF BIOTECHNOLOGY

e-ISSN: 2717-8323

Cilt: 4

Volume: 2

Year: 2023

BULLETIN OF BIOTECHNOLOGY

Cilt: 4 Volume: 2 Year: 2023

Published Biannually

Editor in Chief

Assoc. Prof. Dr. Muhammet DOĞAN

Editor (Associate)

Assoc. Prof. Dr. Demet DOĞAN

Editorial Board

Prof. Dr. Ahmed IMTIAJ	University of Rajshahi, Bangladesh
Prof. Dr. Handan UYSAL	Atatürk University, Turkey
Prof. Dr. Ümmühan ÖZDEMİR ÖZMEN	Gazi University, Turkey
Prof. Dr. Canan CAN	Gaziantep University, Turkey
Prof. Dr. Serap DERMAN	Yıldız Technical University, Turkey
Prof. Dr. Gül ÖZYILMAZ	Mustafa Kemal University, Turkey
Prof. Dr. Tülin ARASOĞLU	Yıldız Technical University, Turkey
Prof. Dr. Thanigaivelan RAJASEKARAN	Muthayammal Engineering College, India
Assoc. Prof. Dr. Huseyin TOMBULOĞLU	Dammam University, Saudi Arabia
Assoc. Prof. Dr. Murat DİKİLİTAŞ	Harran University, Turkey
Assoc. Prof. Dr. Yuliia OLEVSKA	Dnipro University of Technology, Ukraine
Dr. Waseem MUSHTAQ (PhD)	Aligarh Muslim University, India

Corresponding Address

Karamanoğlu Mehmetbey University, Faculty of Health, Sciences, Department of Nutrition and Dietetics,
Karaman, Turkey

E-mail: mtdogan1@gmail.com

Web: <https://www.dergipark.org.tr/biotech>

Owner / Publisher

Assoc. Prof. Dr. Muhammet DOĞAN

This journal is peer-reviewed and published twice (June, December) a year.

All responsibility of the articles belongs to the authors.

e-ISSN 2717-8323

BULLETIN OF BIOTECHNOLOGY

e-ISSN 2717-8323

Cilt: 4 Volume: 2 Year: 2023

Contents

Research Articles

Investigation of the effect of different culture conditions on recombinant protein production 42 - 48

İlkgül AKMAYAN

The effect of curcumin on the necroptosis signaling pathway in colon cancer cells 49-53

Şevval HAS, Alp Can TUNCER, İbrahim BOZGEYİK, Haydar BAĞIŞ, Esra BOZGEYİK

Removal of Copper (II) from Mining Waste Water by Adsorption onto Activated Carbons Produced from Hazelnut Shell 54 - 61

Pınar BOZBEYOĞLU

Investigation of the antioxidant and antibacterial effects of fermented *Cornus mas* and *Rubus sanctus* fruits 62 - 67

Derya ÜNAL, Tuba SEVİMOĞLU

Erratum: Microwave-assisted Green Biosynthesis of Gold Nanoparticles from *Eriobotrya Japonica* Leaf Extract 68

Gönül SERDAR

Review Articles

Challenges in optimizing 3D scaffold for dentin-pulp complex regeneration 69-74

Rola ZAHEDAH, Bircan DİNÇ

Bulletin of Biotechnology

Investigation of the effect of different culture conditions on recombinant protein production

İlkgül Akmayan¹ , Tülin Özbek^{2*} 

¹Department of Molecular Biology and Genetics, Graduate School of Natural and Applied Sciences, Yıldız Technical University Esenler, 34220, Istanbul, Turkey.

²Department of Molecular Biology and Genetics, Faculty of Arts and Sciences, Yıldız Technical University, Esenler, 34220, Istanbul, Turkey

*Corresponding author : ozbektulin@gmail.com

Orcid No: <https://orcid.org/0000-0001-6858-7045>

Received : 31/12/2022

Accepted : 06/08/2023

Abstract: After the COVID-19 pandemic, vaccine production technologies have become the focus of attention of researchers. As a matter of fact, recombinant protein-based antigen production, which is one of them, has taken its place in the first place. Proteins obtained by recombinant DNA technology are used in many industrial areas, especially vaccine applications, due to their reliability. Therefore, it is very important to produce targeted recombinant proteins in large quantities. This study, for the high amounts production of Omp25 protein, which is used as a vaccine candidate against brucellosis, in laboratory conditions, is aimed to reveal the effects of conditions that are the pre-culturing process, inoculation in LB or TB media, denatured or native purification, culturing with/without IPTG. All the results were analyzed by SDS-PAGE, confirmed Western Blot, and the total protein amounts were measured Bradford method. According to the results, Omp25 protein could not be obtained under native purification conditions in both cultures without induction, but it was observed under denatured conditions. This result can be explained that the protein in the cell is either misfolded or incorporated into the membrane. The amount of protein appears to be much higher in the presence of the inducer in both media inoculated with the starter pre-culture compared to the overnight pre-culture; 8.79 mg and 39.4 mg from 1 L culture, respectively. Additionally, as expected, the addition of IPTG increased the amount of protein, approximately one-and-a-half-fold for LB and about three-fold for TB. Finally, it was observed that TB medium provided higher protein production than LB, which can be explained by the presence of glycerol and high yeast extract in the medium. Although our study contains results that will attract the attention of vaccine industry, it should be kept in mind that all process should always be optimized depending on the structure of the targeted protein and thus the production amount can be further increased.

Keywords: Recombinant protein; protein amount; culture condition; Omp25

© All rights reserved.

1 Introduction

The popularity of recombinant protein-based vaccine production, which is among the biotechnology topics, has increased even more after the COVID-19 pandemic (Hortsch and Weuster-Botz 2011; Hu et al. 2022; Huleani et al. 2022). The main purpose of the recombinant protein industry, which acts in many different fields such as health (vaccine, diagnosis, treatment), environment, food, and agriculture, is to obtain protein in high quantity and efficiency without reducing its quality. Due to the different structural properties of recombinant proteins, it is necessary to establish specific optimization conditions for each protein. For this, first of all, the appropriate expression system must be determined. Different heterologous hosts have been used to produce the recombinant protein efficiently. However, current research contains with the *E. coli* host, which is the best-known and most widely used (Anné et al. 2012; Packiam et al. 2020).

Recombinant protein production in *E. coli* began in 1977 with somatostatin for the first time. Nowadays, protein production studies have accelerated actively after the COVID-19 pandemic in 2019 (Jiang et al. 2020, Overton 2014, Yao et al. 2022). After host selection, the growth medium formulation for high protein production should be determined, which usually results in a preference for those containing yeast extract and hydrolyzed protein (Danquah and Forde 2007). In addition, a carbon-energy source (glucose, glycerol, or other sugars) and a nitrogen source are needed for medium formulations. Therefore, Luria Bertani (LB) and Terrific Broth (TB) are chosen as the most suitable media for recombinant protein production (Coskun et al. 2022, Thongbhubate et al. 2021). Another important parameter is the identification of the inducer. Although isopropyl β -D-thiogalactopyranoside (IPTG) is frequently used, it should be noted that the inducer is chosen in conjunction with the

designed vector. Apart from these, modification of the target DNA and vector, determination of the host according to the protein structure (*E. coli* BL21(DE3), BL21(DE3) pLysS, Rosetta™ (DE3) and derivatives, SHuffle® T7 Express and derivatives, CyDisCo, BL21-AI, Tuner (DE3) and derivatives, Lemo21 (DE3), SixPack, Mutant56 (DE3)), optimization of culture parameters such as temperature, time, bacterial density are other factors that directly affect the amount of recombinant protein (Hemamalini et al. 2020; Papanephytou and Kontopidis 2014; Rosano and Ceccarelli 2014). In addition to high production, high recovery of recombinant proteins is also important in the efficiency of production. Therefore, different parameters such as resin type, solvent, pH, buffer system, protein structure and ionic strength should be considered in the purification optimization of recombinant proteins (Coskun et al. 2022).

The Omp25 protein, chosen as a representative model for effective protein production in this investigation, constitutes a hydrophobic and antigenic protein located in the outer membrane of *Brucella abortus*. This protein holds significant promise as a candidate molecule for vaccine research. Brucellosis is an infectious zoonotic illness caused by the *Brucella abortus* and *B. melitensis*, also termed Maltese fever, Mediterranean fever, and fluctuating fever (Yumuk and O'callaghan 2012). Brucellosis affects the gastrointestinal, muscle/joint, neurological, cardiovascular, pulmonary, genitourinary, and hematological systems, as well as the skin, ophthalmic, and endocrinological systems (Çelebi and Hacimustafaoglu 2004).

Based on this information, in this study, the high and efficient production of the rOmp25 protein was evaluated by various factors, which include the preculture procedure, LB or TB media usage, denatured or native purification, and IPTG induction.

2 Materials and Method

2.1 Bacterial strains

B. abortus strain, endemic to the Erzurum Region of Turkey, was grown for three days at 37 °C in blood agar medium under microaerophilic (10% CO₂) conditions (Baily et al. 1992). This strain exists in the culture collection of the Microbiology Laboratory at the Department of Molecular Biology and Genetics, Yıldız Technical University.

2.2 Amplification, Cloning and Transformation

Genomic DNA of bacteria was isolated using the GeneDireX genomic DNA isolation kit (Catalog number: NA023-0100). The forward primer (5'-CACCCGACTCTTAAGTCTCTCGTAAT-3') and the reverse primer (5'-GAAGTTGTAGCCGATGCC-3') were used to amplify the Omp25 gene. Phusion High-Fidelity DNA Polymerase (Thermo Scientific - F530L) was used to create amplicons. PCR conditions consisted of an initial denaturation at 98 °C for 30 seconds; followed by 30 cycles at 98 °C, 10 s; 61 °C, 30 s; 72 °C, 30 s, and a final extension of 72 °C, 10 min. The Omp25 gene was cloned into the PET102/D-TOPO® expression vector containing thioredoxin, which increases protein solubility. After cloning

positive plasmids were transformed into *E. coli* BL21 by the heat shock method (Froger and Hall 2007), the confirmation was performed by colony PCR and sequence analysis (Clustal Omega) (Atabey et al. 2021).

2.3 The optimization of protein expression with different parameters

The flow chart in Figure 1 depicts various factors used to enhance the quantity of recombinant Omp25 protein. These factors include the incubation time of *E. coli* BL21 cells in the LB medium for pre-culture, the choice of LB or TB as the main culture medium, and with/without IPTG culture conditions.

Both overnight and starter pre-cultures containing different incubation times of *E. coli* BL21 were established using distinct methods in the LB medium. The overnight culture involved incubating a single colony in 5 mL of LB medium within a shaking oven at 37 °C and 200 rpm for one night. The second method, for the starter culture, required cultivating it in 10 mL of LB medium at 37 °C and 200 rpm until the absorbance reached OD₆₀₀ 0.5–0.6 A. Subsequently, the culture was divided into Eppendorf tubes, subjected to centrifugation at maximum speed for 5 minutes, the supernatant was discarded, and the resulting pellet was stored at -20 °C. (Research 1998).

LB and TB mediums with different contents were evaluated separately as the main medium. Briefly, LB medium was prepared with ampicillin (0.1 g/L), tryptone (10.0 g/L), yeast extract (5.0 g/L), NaCl (5 g/L). Also, TB medium contained ampicillin (0.1 g/L), tryptone (12.0 g/L), yeast extract (24.0 g/L), glycerol (5 g/L), K₂HPO₄ (12.54 g/L), and KH₂PO₄ (2.31 g/L) (Mühlmann et al. 2017, Zhang et al. 2019). The overnight pre-culture (1:100, v/v) or starter pre-culture (2:100, v/v) was introduced into the prepared LB or TB medium. These cultures were incubated in a shaking incubator at 37 °C 200 rpm until 0.5-0.7 OD₆₀₀ and 1-1.5_A were reached for LB and TB media, respectively. After that, 0.5 mM IPTG was added to the only determining cultures and the cultures incubated in a shaking incubator at 22 °C and 200 rpm for 24 hours. At the end of time, they were centrifuged at 6000 rpm for 15 minutes at 4 °C, and the pellets were stored at -80 °C.

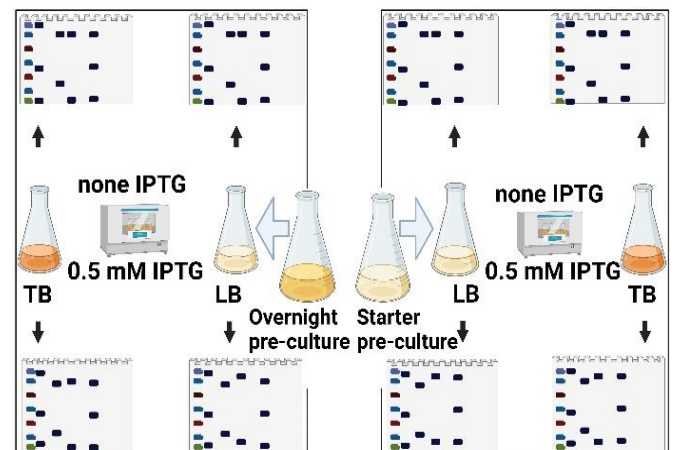


Fig. 1. Flow chart showing optimization of all experimental conditions in this study. (Figure created with BioRender.com)

2.4 Protein purification

Protein purification was carried out by affinity chromatography and rOmp25 binding to Ni-NTA resin by using the His tag located at the N-terminus of the protein was eluted by competing with imidazole. Briefly, the cells removed from -80 °C were kept at room temperature until thawed. After adding 4 ml of lysis buffer, the tubes were sonicated at 65% power for 3 minutes (10 sec. pulse, 20 sec. pause) (Zhang et al. 2018), and centrifuged at 14000 g for 20 minutes at 4 °C (Beckman Allegra X-30 -C650 rotor). For purification at native condition, the supernatant was loaded into spin columns containing HisPur™ Ni-NTA resin by mixing an equal volume of equilibration buffer (0.68 g/L imidazole, 17.55 g/L NaCl, 0.454 g/L NaH₂PO₄, 2.754 g/L Na₂HPO₄, pH 7.4). After the loaded colon was incubated at 4 °C about one hour, it was centrifuged at 700 g for 2 minutes at 4 °C and added the wash buffer (1.702 g/L imidazole, 17.55 g/L NaCl, 0.454 g/L NaH₂PO₄, 2.754 g/L Na₂HPO₄, pH 7.4). After this process is repeated three times, the purification stage was finalized by adding elution buffer (17.7 g/L imidazole, 17.55 g/L NaCl, 0.454 g/L NaH₂PO₄, 2.754 g/L Na₂HPO₄, pH 7.4) to the colon. To achieve denatured conditions for protein purification from the pellet, 8 M urea (480 g/L) was introduced into the solutions. Protein fractions were collected in 1 mL of elution buffer. (Cloeckert et al. 1996a, Cloeckert et al. 1996b).

2.5 Protein analysis

The purified proteins were analyzed by SDS-PAGE for their molecular size, then confirmed by Western blotting and the protein amount was determined using the Bradford test. Briefly, the proteins in the elution buffer were boiled at 96 °C for 5 min after mixing with 5X loading buffer containing 5% (v/v) β-mercaptoethanol and glycerol. Denatured samples were loaded in equal volumes (20 μl) on 12% SDS-PAGE gels. After electrophoresis, the gels were stained with Coomassie Blue (Naseri et al. 2022).

For western blotting, rOmp25 was transferred to a nitrocellulose membrane for 30 minutes at 25 V/1A using the Trans-Blot® Semi-Dry system. The membrane was blocked with a 5% milk solution in PBS-Tween-20. After blocking, the membrane was incubated with the primary His-probe antibody (H-3): sc-8036 (1:250) at 4 °C overnight. At the end of the period, the membrane was washed three times with PBS-Tween 20 and incubated for 2 hours in 5% milk powder (1:5000) HRP-conjugated goat anti-mouse IgG (H+L) secondary antibody (Invitrogen, MA, ABD). After washing in PBS Tween-20, they were treated with 3,3'-diaminobenzidine (DAB)/H₂O₂ for a few minutes to observe the protein band (Tiwari et al. 2011, Woodward et al. 1985).

In the Bradford method, the eluant was added to the microplate containing 250 μl of 1x dye reagent, and the plate was incubated for at least 5 minutes in the dark at room temperature. Then, the microplate was measured in triplicate at 595 nm using a spectrophotometer. (Khrantsov et al. 2021).

3 Results and Discussion

3.1 Amplification, Cloning and Transformation

Omp25 (642 bp) was successfully cloned into the expression vector pET102/D-TOPO. The Omp25 gene sequence was aligned with other Omp25 sequences reported using BLAST and Clustal Omega for homology searches. The Omp25 gene, which was taken from *B. abortus* biovar 3 (Erzurum, Turkey), was found to be identical to gene ID: 3787431, (accession no. AM040264). It also showed higher sequence similarity to other *Brucella* spp. (data not shown).

3.2 Determining optimum parameters for protein expression

The optimization conditions in this study were overnight or previously prepared starter culture as beginner culture, culturing with 0.5 mM IPTG or non-IPTG, and LB or TB medium usage, protein purification in native or denaturing conditions. Firstly, The fusion rOmp25 (41 kDa) protein was successfully produced by purification under denatured conditions from expression cultures (LB-TB) separately initiated with overnight and starter pre-cultures, with IPTG or without IPTG.

In Figure 2, the parameters applied in LB and TB media are shown comparatively by SDS-PAGE analysis. In Figure 2, the characteristic band profile (Lines A.1–6, B.1–4) of the rOmp25 protein obtained only in denatured conditions rather than in native conditions without IPTG (A-B. Lines 7–10) is clearly shown. The band density observed as a result of the comparison of the parameters applied for the denatured Omp25 protein is noteworthy (A. Lines 11–17, B. Lines 12–19).

Optimization parameters for overexpression of the rOmp25 protein are shown in Figure 3, which were confirmed by western blot after SDS-PAGE analysis. The band profile of the denatured rOmp25 protein is more intensely observed in starter pre-culture rather than overnight pre-culture, and in TB compared to LB. As shown in Figures 2–3, the band intensities of rOmp25 match the Bradford results. In addition, it was shown that the starter pre-culture reached a high protein amount (3.94 mg/mL) at TB medium with 0.5 mM IPTG (Table 1). In Figure 4, the effect of different absorbance values on the amount of protein is illustrated with SDS-PAGE images.

In the literature, the amount of rOmp25 produced in LB medium with overnight starter culture was found to be 50 µg/mL (Ahmed et al. 2015) and 220 µg/mL. (Yousefi et al. 2016) In our study, the fact that the protein amount increased to 0.965 mg/ml for LB and 3.2 mg/ml for TB in a single elution tube with the starter pre-culture application indicates the success in optimization.

The rDME-E protein purified under denaturing conditions was produced in amounts of 10.37 mg/L, 16.53 mg/L, 17.31 mg/L and 21.65 mg/L in LB, TB, SB and TY media, respectively, after the addition of 0.5 mM IPTG and overnight

preculture (Tripathi et al. 2009). In our study, the fact that higher protein (39.4 mg/L) was produced in TB medium with starter pre-culture emphasises the importance of beginner culture.

It is known that the use of IPTG as an inducing agent increases protein yield. This confirms that saturation of the Sec-translocon capacity is directly related to the production efficiency of membrane proteins, as stated in the study by Zhe Zhang et al., and that saturation cannot be reached in the absence of the inducer. (Zhang et al. 2015).

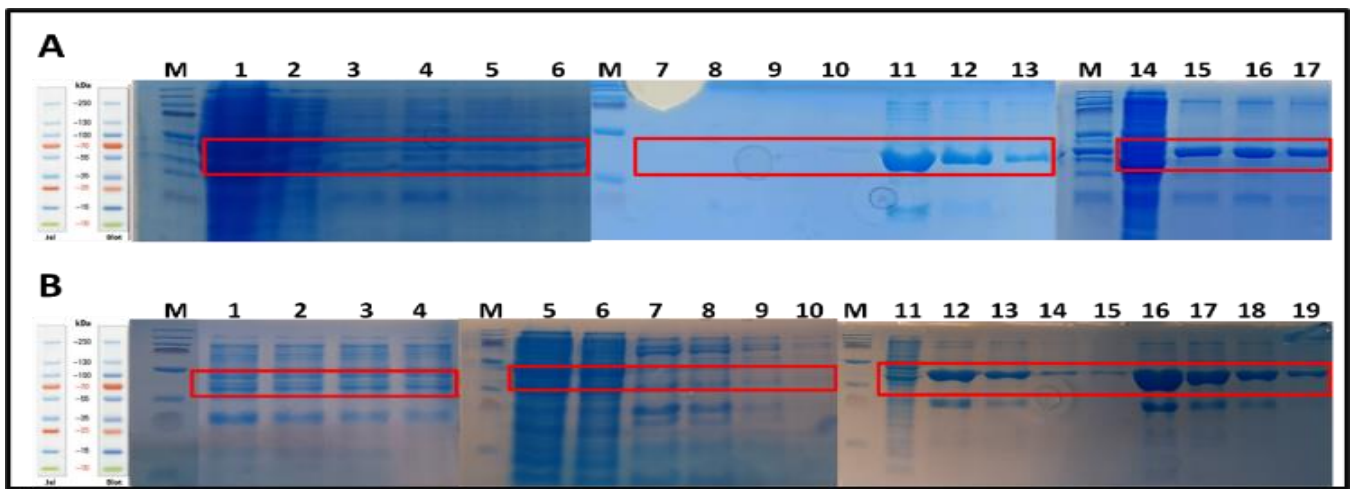


Fig. 2. SDS-PAGE images illustrating the outcomes of the evaluated parameters for LB (A) and TB medium (B).
 A) Line M: Marker; Lines 1-6: The rOmp25 proteins were extracted following the conditions given in Table 1 parameter 7; flow-through, wash, and elution fractions, respectively; Lines 7–10: the elution fractions purified under native conditions after overexpression using overnight pre-culture and without IPTG, elution fractions 1-4, respectively (not rOmp25); Lines 11-13: The rOmp25 proteins were isolated following the procedure outlined in Table 1, parameter 2; elution fractions 1-3 respectively; Lines: 14-17: rOmp25 protein extracted from cells under Table I, parameter 1; cell crude extract, elution fractions 1-3, respectively.
 B) Line M: Marker; Lines 1-4: The rOmp25 proteins were extracted as described in Table 1 parameter 5; elution fractions 1-4, respectively; Lines 5-10: Elution fractions purified under native conditions after overexpression using overnight pre-culture and without IPTG (not-rOmp25), respectively, flow-through, wash, elution fractions; Lines 11-15: The condition of the fourth parameter product rOmp25, as described in Table 1 parameter 3, is cell crude extract, elution fractions 1-4, respectively; Lines 16-19: Elution fractions obtained in the 4th parameter conditions in Table 1, elution fractions 1-4, respectively.

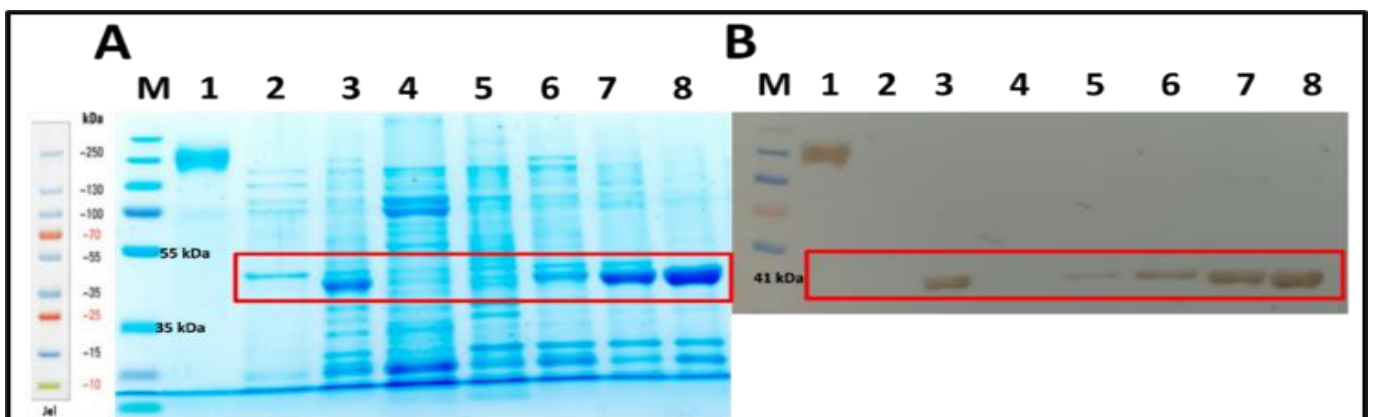


Fig. 3. Western blot image with SDS-PAGE analysis containing all parameters. A-B) Line M: Marker; Line 1: Commercial protein; Line 2: rOmp25 not obtainable under native conditions (overnight pre-culture-LB); Line 3: rOmp25 (Parameter 7th, Table 1); Line 4: rOmp25 not obtainable under native conditions (overnight pre-culture-TB); Line5: rOmp25 (Parameter 5th, Table 1); Line 6: rOmp25 (Parameter 1st, Table 1); Line 7: rOmp25 (Parameter 2nd, Table 1); Line 8: rOmp25 Parameter 3rd, Table 1).

Figure 4 shows the effect of bacterial absorbance value on protein yield during addition of inducing agent in different environments. Expression results in TB medium supplemented with IPTG after starter pre-culture indicate the highest amount of protein. When not induced, the amount of protein appears to be reduced by about half. This situation is similar for LB. In addition, both protein content and protein yield increase in TB, which is rich in yeast extract and phosphate salts, depending on the increase in cell density (Tripathi et al. 2008).

Table 1 Comparative total protein of purified denaturing conditions rOmp25 protein in culture

Parameters	Overnight/Starter pre-culture	IPTG (mM)	OD ₆₀₀ (A)	Medium	Total Protein Amount (mg/L)
1	Overnight	0.5	0.58	LB	3.05
2	Starter	0.5	0.6	LB	8.79
3	Overnight	0.5	1.1	TB	21.8
4	Starter	0.5	1.1	TB	39.4
5	Overnight	-	1	TB	9.8
6	Starter	-	1	TB	14.16
7	Overnight	-	0.58	LB	2.2
8	Starter	-	0.59	LB	5.9

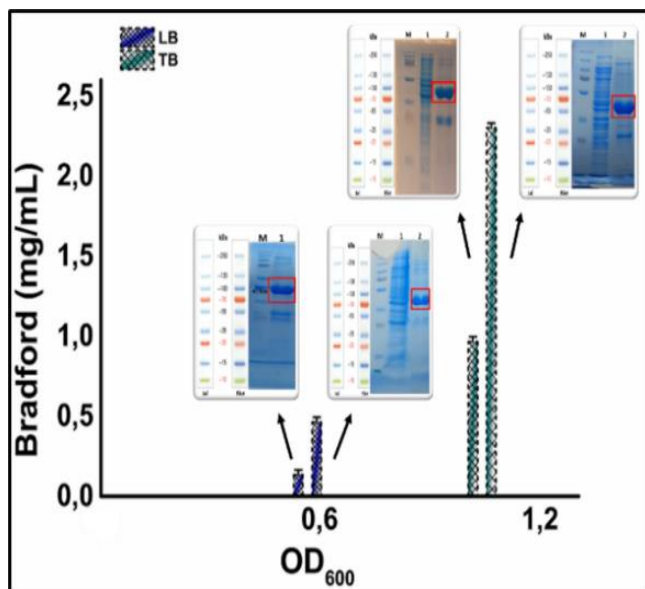


Fig. 4. Demonstration of the effect of bacterial growth and pre-culture conditions on protein yield with SDS-PAGE images.

*Short peak; The effect of LB (0.5-0.6A) and TB (1-1.5A) values on overnight pre-culture protein yield,

*Long peak; The effect of LB (0.5-0.6A) and TB (1-1.5A) values on starter pre-culture protein yield.

It is stated in the literature that a single dose of rOmp25 used for vaccine purposes is administered to experimental animals in the range of 0.25 - 40 μ g (Goel and Bhatnagar 2012, Ma et al. 2015, Goel et al. 2013, Yousefi et al. 2018) and Therefore, the protein amounts obtained after the optimization in this study provide an advantage to vaccine research in terms of time, cost and workload. In addition, it is also important that the amount of rOmp25 produced in our study meets the desired protein amount (5 mg/ml) (Goel et al 2013) for different strategies in nanotechnological methods, which is the last point reached by vaccination technologies.

Conclusion

Consequently, rOmp25, known as the outer membrane protein, was produced in high amount in the presence of inducer in TB mother medium started with starter preculture, and its recovery was much more efficient under denaturation conditions. Moreover, in protein expression induced by overnight preculture, TB medium produced much higher rOmp25 than LB. Finally, another critical factor that significantly increased the amount of protein was the presence of IPTG (isopropyl β -D -1-thiogalactopyranoside) in the expression medium.

Acknowledgements

The authors are grateful to the Scientific and Technological Research Council of Turkey (TUBITAK, “2247/C STAR COVID-19”) and The Council of Higher Education of the Republic of Turkey (YOK, “YOK100/2000”) for providing the first author with a research scholarship. This report involves a part of İlkül Akman's doctoral thesis. This work was supported by Yıldız Technical University Scientific Research Projects Coordination Unit. Project number: FBA-2022-4648. The authors thank Tuğba ATABEY for her contributions to the rOmp25 protein study.

Authors' contributions: İA: Investigation, methodology, formal analysis, writing-original draft, writing-review& editing, visualization. TÖ: Investigation, writing-original draft, review&editing, supervision.

Conflict of interest disclosure:

The authors of this study declare that they have no conflict of interest.

References

- Anné J, Maldonado B, Van Impe J, Van Mellaert L, Bernaerts K (2012) Recombinant protein production and streptomycetes. *J of biotec* 158:159-167. doi: 10.1016/j.jbiotec.2011.06.028
- Atabey T, Acar T, Derman S, Ordu E, Erdemir A, Taşlı P N, Gür G K, Şahin F, Güllüce M, Arasoğlu T (2021) In Vitro Evaluation of Immunogenicity of Recombinant OMP25 Protein Obtained from Endemic *Brucella abortus* Biovar 3 as Vaccine Candidate Molecule Against Animal Brucellosis. *Protein and Pept Let* 28:1138-147. doi:https://doi:10.2174/0929866528666210615104334

- Ahmed IM, Khairani-Bejo S, Hassan L, Bahaman AR, Omar RA (2015) Serological diagnostic potential of recombinant outer membrane proteins (rOMPs) from *Brucella melitensis* in mouse model using indirect enzyme-linked immunosorbent assay. *BMC Vet Res* 11:275 <https://doi.org/10.1186/s12917-015-0587-2>
- Baily G, Krahn J, Drasar B, Stoker N (1992) Detection of *Brucella melitensis* and *Brucella abortus* by DNA amplification. *J Trop Med Hyg* 95:271-275.
- Cloekaert A, Verger J-M, Grayon M, Zygmunt M S, Grépinet O (1996a) Nucleotide sequence and expression of the gene encoding the major 25-kilodalton outer membrane protein of *Brucella ovis*: evidence for antigenic shift, compared with other *Brucella* species, due to a deletion in the gene. *Infect Immun* 64:2047-2055. doi: 10.1128/iai.64.6.2047-2055.1996
- Cloekaert A, Zygmunt M, Bezard G, Dubray G (1996b) Purification and antigenic analysis of the major 25-kilodalton outer membrane protein of *Brucella abortus*. *Res Microbiol* 147:225-235. doi: [https://doi.org/10.1016/0923-2508\(96\)81383-0](https://doi.org/10.1016/0923-2508(96)81383-0)
- Coskun KA, Yurekli N, Abay EC, Tutar, M., Al, M, Tutar, Y. (2022). Structure-and Design-Based Difficulties in Recombinant Protein Purification in Bacterial Expression. *Protein Detection*. 3.
- Çelebi S, Hacimustafaoğlu M, (2004). Bruselozis. *Güncel Pediatri*, 2(1), 39-43.
- Danquah M K, Forde GM (2007) Growth medium selection and its economic impact on plasmid DNA production. *J Biosci Bioeng* 104:490-497. doi: 10.1263/jbb.104.490
- Froger A, Hall JE (2007) Transformation of plasmid DNA into *E. coli* using the heat shock method. *J Vis Exp* 6:e253. doi: 10.3791/253
- Goel D, Bhatnagar R, (2012). Intradermal immunization with outer membrane protein 25 protects Balb/c mice from virulent *B. abortus* 544. *Mol Immun* 51: 159 -168. doi:10.1016/j.molimm.2012.02.126
- Goel D, Rajendran V, Ghosh PC, Bhatnagar R, (2013). Cell mediated immune response after challenge in Omp25 liposome immunized mice contributes to protection against virulent *Brucella abortus* 544. *Vaccine*, 31(8), 1231-1237. doi:10.1016/j.vaccine.2012.12.04
- Hemamalini N, Ezhilmathi S, Mercy AA (2020) Recombinant protein expression optimization in *Escherichia coli*: A review. *Indian J Anim Res* 54:653-660. doi: 10.18805/ijar.B-3808
- Hortsch R, Weuster-Botz D (2011) Growth and recombinant protein expression with *Escherichia coli* in different batch cultivation media. *App microbiol biotechnol* 90:69-76. doi: 10.1007/s00253-010-3036-y
- Hu Z, Chen J-P, Xu J-C, Chen Z-Y, Qu R, Zhang L, Yao W, Wu J, Yang H, Lowrie DB (2022) A two-dose optimum for recombinant S1 protein-based COVID-19 vaccination. *Virology* 566:56-59. doi: 10.1016/j.virology.2021.11.011
- Huleani S, Roberts MR, Beales L, Papaioannou EH (2022) *Escherichia coli* as an antibody expression host for the production of diagnostic proteins: significance and expression. *Crit Rev Biotechnol* 42:756-773. <https://doi.org/10.1080/07388551.2021.1967871>
- Jiang H, O'Callaghan D, Ding J-B (2020) Brucellosis in China: history, progress and challenge. *Infect Dis Poverty* 9:101-104. doi: 10.1186/s40249-020-00673-8
- Khramtsov P, Kalashnikova T, Bochkova M, Kropaneva M, Timganova V, Zamorina S, Rayev M (2021) Measuring the concentration of protein nanoparticles synthesized by desolvation method: Comparison of Bradford assay, BCA assay, hydrolysis/UV spectroscopy and gravimetric analysis. *Int J Pharm* 599:120422. <https://doi.org/10.1016/j.ijpharm.2021.120422>
- Ma QL, Liu AC, Ma XJ, Wang YB, Hou YT, Wang ZH (2015). *Brucella* outer membrane protein Omp25 induces microglial cells in vitro to secrete inflammatory cytokines and inhibit apoptosis. *Int J Clin Exp Med*. 15;8(10):17530-5. PMID: 26770344; PMCID: PMC4694244.
- Mühlmann M, Forsten E, Noack S, Büchs J (2017) Optimizing recombinant protein expression via automated induction profiling in microtiter plates at different temperatures. *Microb Cell Factories* 16:1-12. <https://doi.org/10.1186/s12934-017-0832-4>
- Naseri N, Mirian M, Mofid MR (2022) Expression of recombinant insulin-like growth factor-binding protein-3 receptor in mammalian cell line and prokaryotic (*Escherichia coli*) expression systems. *Adv Biomed Res* 11:19. doi: 10.4103/abr.abr_197_20
- Overton TW (2014) Recombinant protein production in bacterial hosts. *Drug Discov Today* 19:590-601. doi: 10.1016/j.drudis.2013.11.008
- Packiam KAR, Ramanan RN, Ooi CW, Krishnaswamy L, Tey BT (2020) Stepwise optimization of recombinant protein production in *Escherichia coli* utilizing computational and experimental approaches. *Appl Microbiol Biotechnol* 104:3253-3266. doi.org/10.1007/s00253-020-10454-w
- Papaneophytou CP, Kontopidis G (2014) Statistical approaches to maximize recombinant protein expression in *Escherichia coli*: a general review. *Protein Expr Purif* 94:22-32. doi: 10.1016/j.pep.2013.10.016
- Ratnaningsih E, Sukandar SI, Putri RM, Kadja GT, Wenten IG (2022) Optimization of haloacid dehalogenase production by recombinant *E. coli* BL21 (DE3)/pET-hakp1 containing haloacid dehalogenase gene from *Klebsiella pneumoniae* ITB1 using Response Surface Methodology (RSM). *Heliyon* e11546. doi: 10.1016/j.heliyon.2022.e11546
- Research PW (1998) *E. Coli Culture for Protein Expression*. In: *Investigating the Biochemistry & Cellular Physiology of NHE1EST*. [online] Available at. <https://home.sandiego.edu/~josephprovost/E.%20Coli%20protein%20expression%20protocol.pdf> Accessed: 08 March 2022
- Rosano GL, Ceccarelli EA (2014) Recombinant protein expression in *Escherichia coli*: advances and challenges. *Front Microbiol* 5:172. <https://doi.org/10.3389/fmicb.2014.00172>
- Thongbhuate K, Irie K, Sakai Y, Itoh A, Suzuki H (2021) Improvement of putrescine production through the arginine decarboxylase pathway in *Escherichia coli* K-12. *AMB Express* 11:1-13. <https://doi.org/10.1186/s13568-021-01330-5>
- Tiwari AK, Kumar S, Pal V, Bhardwaj B, Rai GP (2011) Evaluation of the recombinant 10-kilodalton immunodominant region of the BP26 protein of *Brucella abortus* for specific diagnosis of bovine brucellosis. *Clin Vaccine Immunol* 18:1760-1764. doi: 10.1128/01.05159-11
- Tripathi NK, Babu JP, Shrivastva A, Parida M, Jana AM, Rao PL (2008) Production and characterization of recombinant dengue virus type 4 envelope domain III protein. *J Biotechnol* 134:278-286. doi: 10.1016/j.jbiotec.2008.02.001

- Tripathi N K, Shrivastva A, Biswal KC, Rao, PVL (2009). METHODS: Optimization of culture medium for production of recombinant dengue protein in *Escherichia coli*. *Indust. Biotech.* 5(3), 179–183. doi:10.1089/ind.2009.3.179
- Woodward M, Young Jr W, Bloodgood R (1985) Detection of monoclonal antibodies specific for carbohydrate epitopes using periodate oxidation. *J Immunol Methods* 78:143-153. doi: 10.1016/0022-1759(85)90337-0
- Yao M, Guo X, Wu X, Bai Q, Sun M, Yin D (2022) Evaluation of the Combined Use of Major Outer Membrane Proteins in the Serodiagnosis of Brucellosis. *Infect Drug Resist* 4093-4100. doi: 10.2147/IDR.S372411
- Yousefi S, Abbassi-Daloi T, Sekhavati MH, & Tahmoorespur M, (2018). Evaluation of immune responses induced by polymeric OMP25-BLS *Brucella* antigen. *Microb Pathog* 115: 50–56. doi:10.1016/j.micpath.2017.12.045
- Yousefi S, Tahmoorespur M, Sekhavati MH, (2016) Cloning, expression and molecular analysis of Iranian *Brucella melitensis* Omp25 gene for designing a subunit vaccine, *Res pharm* 11(5) 412. doi: 10.4103/1735-5362.192493
- Yumuk Z, O'Callaghan D (2012). Brucellosis in Turkey—an overview. *International J Infect Dis* 16(4): e228-e235
- Zhang B, Gu H, Yang Y, Bai H, Zhao C, Si M, Su T, Shen X (2019) Molecular mechanisms of AhpC in resistance to oxidative stress in *Burkholderia thailandensis*. *Front Microbiol* 10:1483. <https://doi.org/10.3389/fmicb.2019.01483>
- Zhang W, Lu J, Zhang S, Liu L, Pang X, Lv J (2018) Development an effective system to expression recombinant protein in *E. coli* via comparison and optimization of signal peptides: expression of *Pseudomonas fluorescens* BJ-10 thermostable lipase as case study. *Microb Cell Factories* 17:1-12. <https://doi.org/10.1186/s12934-018-0894-y>
- Zhang Z, Kuipers G, Niemiec Ł, Baumgarten T, Slotboom DJ, de Gier J-W, Hjelm A (2015) High-level production of membrane proteins in *E. coli* BL21 (DE3) by omitting the inducer IPTG. *Microb Cell Factories* 14:1-11. <https://doi.org/10.1186/s12934-015-0328-z>

Bulletin of Biotechnology

The effect of curcumin on the necroptosis signaling pathway in colon cancer cells

Sevval Has¹, Alp Can Tuncer¹, Ibrahim Bozgeyik², Haydar Bagis³, Esra Bozgeyik^{4*}

¹Department of Medical Services and Techniques, Vocational School of Health Services, Medical Laboratory Techniques Program, Adiyaman University, Adiyaman, Turkey

²Department of Medical Genetics, Faculty of Medicine, Adiyaman University, Adiyaman, Turkey

³Department of Medical Genetics, Faculty of Medicine, Adiyaman University, Adiyaman, Turkey

⁴Department of Medical Services and Techniques, Vocational School of Health Services, Adiyaman University, Adiyaman, Turkey

*Corresponding author: ebozgeyik@adiyaman.edu.tr; gyk.esra@gmail.com

Orcid No: <https://orcid.org/0000-0002-8726-3182>

Received : 11/09/2023

Accepted : 26/10/2023

Abstract: Colon cancer is the one of the most common types of cancer in humans. A sedentary lifestyle, increasing obesity and the consumption of food additives favor the development and occurrence of colon cancer. It is emphasized that curcumin, a yellow compound isolated from the turmeric plant, is important in preventing cancer. Studies have shown that curcumin has an anticancer effect by driving cancer cells into apoptosis, but studies showing its effect on necroptosis are inconclusive. Necroptosis is a form of programmed cell death mediated by RIP proteins and has been shown to play an important role in cancer. This study aims to determine the effect of curcumin on the necroptosis signaling pathway. For this purpose, HT-29 and HCT-116 colon cancer cells were cultured and exposed to different concentrations of curcumin and MTT experiments were performed to determine the effect on cell viability. The expression levels of RIPK1, RIPK3, and MLKL genes, which are markers of necroptosis, were analyzed by real-time PCR. It was found that the expression level of RIPK1, RIPK3, and MLKL genes significantly increased after exposure of HT-29 cells to 50 μ M curcumin. Moreover, the expression of RIPK1 and MLKL genes increased in HCT-116 cells after curcumin administration. Consequently, the current data clearly suggest that curcumin is a prominent driver of necroptotic signaling-mediated colon cancer cell death.

Keywords: Colon cancer; Curcumin; Necroptosis; RIPK1; RIPK3; MLKL

© All rights reserved.

1 Introduction

Cancer is the second-leading public health problem worldwide after cardiovascular diseases. Among the other cancer types, the incidence and mortality of colon cancer is quite high. In addition, studies have shown that colon cancer is mainly characterized by the accumulation of genetic and epigenetic changes (Marley et al. 2016). According to 2020 Global cancer statistics, it was reported that 1.1 million people were diagnosed with colon cancer and 0.58 million people died due to colon cancer (Sung et al. 2021). Also, sedentary lifestyle and increased obesity, low consumption of fibrous food sources and consumption of industrial foods with additives increase the development of colon cancer. Furthermore, according to the World Health Organization, 75-80% of the world's population consumes medicinal plants as their primary source of health care (Verma and Singh 2008). The main reason for this appears to be the anticancer activities of these plant species. In addition, it has been reported that the risk of developing lung, stomach, mouth,

pharynx, esophagus, colon, and rectum cancers is inversely proportional to fruit and vegetable consumption.

Curcumin (1,7-bis(4-hydroxy-3-methoxyphenyl)-1,6-heptadiene-3,5-dione) is a polyphenolic compound isolated from the rhizome of *Curcuma longa* Linn. Accumulating mass of indication suggests that curcumin has antioxidant, anti-inflammatory, anti-bacterial, anti-diabetic, and anti-cancer activities (Selvam et al. 2019). Curcumin has shown to have significant impact on many signaling pathways in cancer cells, which controls various cellular activities. The anticancer activities of curcumin have also been shown in colon cancer cells (Selvam et al. 2019). Curcumin has been demonstrated to show anti-cancer activity in HT-19 colon cancer cells by suppressing colony formation, cell viability, and DLEC1 promoter methylation (Guo et al. 2015). In addition, curcumin has been shown to suppress the level of ATG5 (autophagy related 5) protein in HCT-116 cells, leading to the suppression of autophagosome formation, cellular senescence, and cell cycle arrest (Mosieniak et al.

2012). In addition, studies have shown that curcumin has anticancer activity in other colon cancer cells such as Caco-2, HCT-15, and SW620 (Selvam et al. 2019). However, the effects of curcumin on the necroptosis pathway have not yet been demonstrated and remain elusive.

It is evident that apoptosis acts as a natural barrier against the development of cancer (Hanahan and Weinberg 2011). Also, resistance to apoptosis is an important hallmark of cancer and is often responsible for both tumorigenesis and drug resistance (Hanahan and Weinberg 2011; Johnstone et al. 2002). In addition to studies to overcome resistance to apoptosis, it is of great interest to develop approaches to induce non-apoptotic forms of programmed cell death as alternative therapeutics in cancer (Gong et al. 2019). One of these non-canonical cell death mechanisms is necroptosis. Necroptosis is a distinct form of cell death mechanism because it resembles apoptosis by the presence of a signal transduction pathway and necrosis by cell morphology. Also, necroptosis is a caspase-independent cell death mechanism and has been shown to be associated with the pathobiology of various diseases including cancer. Holler et al. were the first to report RIPK1 (receptor-interacting protein [RIP] kinase 1) as a member of necroptotic signaling pathway (Holler et al. 2000). Activation of RIP1 induces either apoptosis or necroptosis. Necroptotic signaling is initiated when RIP1 phosphorylates RIP3 to induce the activation of MLKL (mixed lineage kinase domain-like protein) (Cho et al. 2009; He et al. 2009; Sun et al. 2012). MLKL is then oligomerized and transported to the plasma membrane, thereby leading to the execution of necroptosis, resulting in necrotic plasma membrane permeability. Subsequently, necroptotic cell death occurs, characterized by swelling of the cell and loss of cell and organelle integrity (Cai et al. 2014; Sun et al. 2012).

It is well documented that curcumin has a wide range of biological activities, especially the anti-cancer activity of curcumin attracts more attention. However, there are few studies demonstrating the effect of curcumin on the necroptosis pathway in colorectal cancer cells. Accordingly, here we aimed to investigate the effect of curcumin on the necroptosis pathway in colon cancer cells.

2 Materials and Method

2.1 Cell culture

HT-29 and HCT-116 colon cancer cells were used for this study. Cells were cultured at 37 °C in a carbon dioxide incubator containing 5% CO² and 95% air. HT-29 and HCT-116 cells were grown in DMEM (Dulbecco's Modified Eagle Medium) supplemented with 10% fetal bovine serum (FBS) and 1% penicillin/streptomycin. Confluent cells were removed with trypsin and centrifuged at 1500 rpm for 5 minutes. After centrifugation, the supernatant was removed, and the cells were homogenized in the medium.

2.2 Cell viability experiments

Cells were plated in 96-well plates at a concentration of 30,000 cells/ml and incubated for 24 hours. After 24 hours, the medium was removed and washed with 1X PBS (phosphate buffered saline). A 400 µM master stock solution was prepared by dissolving powdered curcumin with dimethyl sulfoxide (DMSO). Serial dilutions were then

prepared from the main stock and HT-29 and HCT-116 cells were treated with the different concentrations of 200-100-50-25-12.5-6.25-0 µM curcumin and incubated for 24 hours. Following 24 hours of incubation, supernatants were discarded, and cells were rinsed with 1X PBS. Then, cells were treated with 1 mg/ml MTT (methylthiazolyldiphenyl-tetrazolium bromide) solution and incubated for 45-60 min at 37 °C. After the incubation, the supernatant was withdrawn, and the blue-violet formazan particles were dissolved with DMSO and read in a microplate reader at a wavelength of 570 nm and half maximum inhibitory concentrations were determined accordingly.

2.3 Colony forming assay

Colony formation experiments were carried out to determine the effect of curcumin on colony formation. First, cells were seeded at 1000 cells per well in 12-well plates and incubated for 24 hours. The cells were then exposed to curcumin and kept in the incubator for about 2 weeks. The experiment was terminated when there were approximately 50 cells in each colony. Colonies were then visualized by incubating 1 ml of 0.5% Crystal Violet dye solution at room temperature for 20 minutes. After incubation, wells were rinsed with distilled water until the colonies were visible and the plate was turned upside down and allowed to dry.

2.4 Gene expression analysis

RNA isolation

For gene expression analysis, total RNA was first isolated from cells using the GeneJET RNA Purification Kit (Thermo Scientific, USA) according to the manufacturer's recommendations. To determine the concentrations of the RNA samples, the RNAs were then measured in a NanoDrop 1000 (Thermo Fisher, USA) spectrophotometer and immediately placed in the refrigerator at -80 °C.

cDNA synthesis

The RevertAid First Strand cDNA Synthesis Kit (Thermo Scientific) was used for single-stranded cDNA synthesis from isolated RNA samples. The mixture prepared according to the recommended procedure was exposed to thermal conditions at 25°C for 5 minutes, at 42°C for 60 minutes, and then at 70°C for 5 minutes. The synthesized cDNA was immediately placed on ice and stored at -80°C.

Real-Time PCR

Specific primers for the RIPK1, RIPK3, MLKL, and GAPDH genes were designed to determine their expression levels (Bozgeyik et al. 2023). RealQ Plus 2x Master Mix Green Kit (Amplicon, Denmark) was used to determine gene expressions. The prepared PCR mixtures were subjected to thermal conditions at 95 °C for 15 minutes (1 cycle), at 95 °C for 15 seconds, at 60°C for 30 seconds, and at 72 °C for 30 seconds (40 cycles). At the end of each reaction, melting curve analysis was performed between 55 and 95°C. After the reaction, the Ct value was determined for each sample at an appropriate threshold value. Gene expression level was determined according to the formula $2^{-\Delta Ct}$ ($-\Delta Ct = Ct_{\text{target gene}} - Ct_{\text{references gene}}$).

3 Results

3.1 The effect of curcumin on cell viability and colony forming capabilities of colon cancer cells

To determine the antiproliferative activity of curcumin on HT-29 and HCT-116 colon cancer cells, we used MTT cell viability assay. A dose-dependent effect on cell viability was determined according to the increasing concentrations of curcumin. The minimum inhibitory concentration was determined to be 50 μM in both HT-29 and HCT-116 colon cancer cells (Fig 1). In addition, after the effective dose of curcumin was determined, its effect on colony formation was determined. Moreover, in consistent with the cell viability analysis, colony forming capabilities of colon cancer cells were determined to be dramatically reduced in cells treated with curcumin (Fig 2).

3.2 The effect of curcumin on the necroptosis pathway

To determine the effect of necroptosis in cells exposed to curcumin, the expression level of RIPK1, RIPK3 and MLKL genes was determined by Real-Time PCR. After exposure of HCT-116 cells with 50 μM curcumin, expression levels of RIPK1 ($p=0.0032$) and MLKL ($p=0.0008$) genes were found to be significantly increased compared to control. However, because RIPK3 expression was absent in HCT-116 cells, no change was observed (Fig 3). In addition, expression levels of RIPK1 ($p<0.0001$), RIPK3 ($p<0.0001$) and MLKL ($p=0.0006$) genes were found to increase after exposure of HT-19 cells to 50 μM curcumin (Fig 4). This change in the expression levels of RIPK1, RIPK3, and MLKL genes suggests that curcumin may be an important flavonoid in regulating the necroptosis pathway.

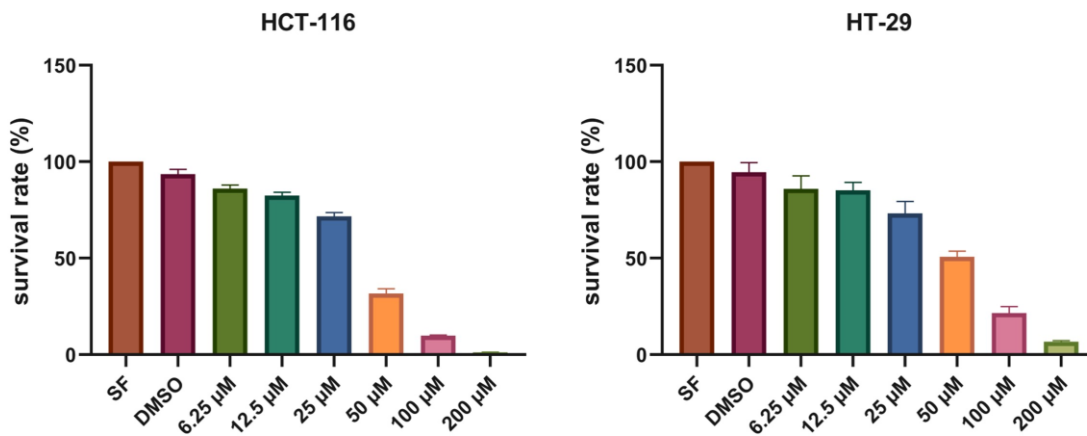


Fig 1. Effect of curcumin on cell viability at different concentrations in HCT-116 and HT-29 colon cancer cells.

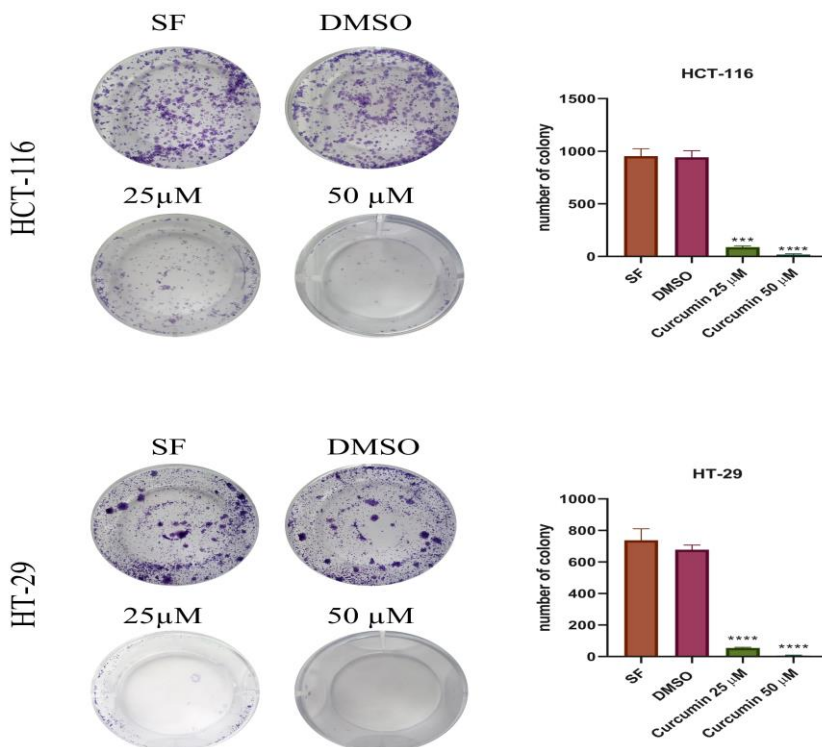


Fig 2. Effect of curcumin on colony forming capabilities of colon cancer cells.

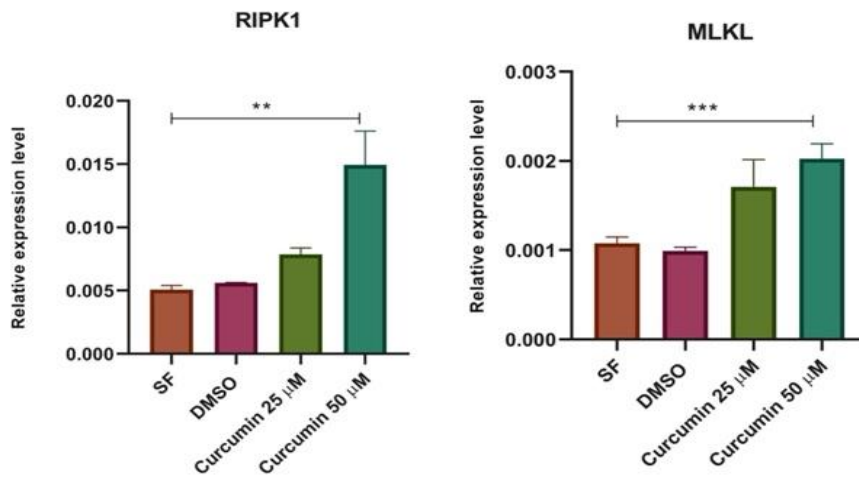


Fig 3. Gene expression changes of RIPK1 and MLKL genes following curcumin administration in HCT-116 cells. ** $p < 0.01$, *** $p < 0.001$.

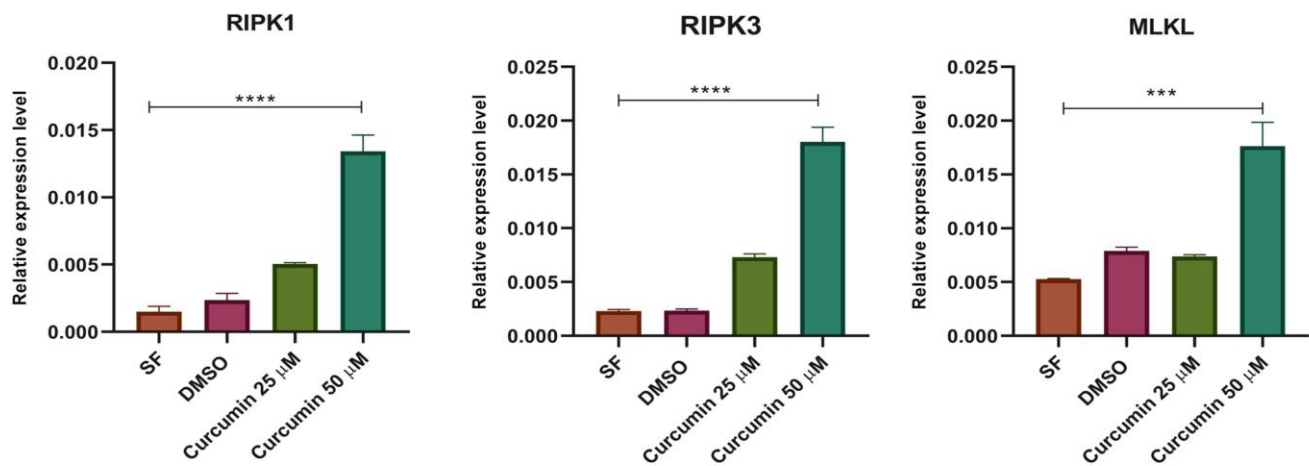


Fig 4. Gene expression changes of RIPK1, RIPK3 and MLKL following curcumin administration in HT-29 cells. *** $p < 0.001$, **** $p < 0.0001$.

4 Discussion

In the present study, necroptotic death of colon cancer cells were found to be significantly induced by curcumin administration. Notably, expression level of RIPK1, RIPK3 and MLKL genes, which are important necroptosis markers, increased significantly when HT-29 colon cancer cell was exposed to curcumin compared to the control group. In addition, curcumin was found to interfere with the proliferation of colon cancer cells by activating the necroptosis signaling pathway in these cells, strongly suggesting that curcumin is a significant regulator of necroptotic cell death mechanism.

Curcumin, which is extracted from the plant *Curcuma longa*, is known to have numerous biological and pharmacological activities. Curcumin has been reported to stimulate cell death pathways such as apoptosis, autophagy, and pyroptosis in many different cancer cells. In a study by Blakemore et al., curcumin was shown to disrupt the cell cycle progression by inducing G2/M cell cycle arrest in various colon cancer cells (Blakemore et al. 2013). In addition, curcumin treatment has been shown to cause abnormal mitotic spindle formation and DNA damage. In addition, curcumin has been shown to dose-dependently suppress cell proliferation and induce p53-

mediated apoptosis in HT-29 and HCT-116 cells (Watson et al. 2010), increase the expression of pro-apoptotic genes such as BAD, BAX, and decrease the expression of anti-apoptotic BCL2 (Guo et al. 2013; Rana et al. 2015). Another biological feature of curcumin is its effect on epithelial mesenchymal transition and invasion and metastasis of cancer cells. In both in vivo and in vitro studies, it has been reported that curcumin has anti-metastatic activity in colon cancer cells by causing downregulation of the expression of the transcription factor Sp-1 and the cell adhesion component FAK and upregulation of the epithelial marker E-cadherin (Chen et al. 2013). In a study by Chen et al., it was reported that N-cadherin, Vimentin, Wnt3a, Snail1, Twist genes were downregulated in SW480 colon cancer cells depending on curcumin concentration (Chen et al. 2020). Despite this wide range of biological activities, studies showing the effect of curcumin on the necroptosis pathway in colon cancer cells are still unclear. In a study by Lee et al, curcumin was shown to target both apoptosis and necroptosis by causing DNA damage, increased reactive oxygen species production, and mitochondrial dysfunction in PC -3 prostate cancer cells (Lee et al. 2021). In HUVECs, a curcumin analog has also shown a necroptotic effect and induction of cell death by the curcumin analog could be partially reversed by administration of Necrostatins (Liu et al. 2019).

5 Conclusion

Remarkably, in our study, curcumin was shown to stimulate necroptosis by increasing the expression of RIPK1, RIPK3, and MLKL genes, especially in HT-29 colon cancer cells. In conclusion, present findings strongly indicate that curcumin is a significant driver of colon cancer cell death mediated by necroptotic signaling.

Acknowledgements

This work was funded by The Scientific & Technological Research Council of Turkey (TUBITAK) (Grant No: 1919B012202271).

Authors' contributions: SH: Methodology, Data curation, Writing - review & editing ACT: Methodology, Writing - review & editing IB: Methodology, Data curation, Writing - original draft, Writing - review & editing HB: Methodology, Writing - review & editing. EB: Conceptualization, Supervision, Methodology, Data curation, Writing - original draft, Writing - review & editing.

Conflict of interest disclosure: The authors of this study declare that they have no conflict of interest.

References

- Blakemore LM, Boes C, Cordell R, Manson MM (2013). Curcumin-induced mitotic arrest is characterized by spindle abnormalities, defects in chromosomal congression and DNA damage. *Carcinogenesis* 34:351-360
- Bozgeyik E, Bagis H, Bozgeyik I, Kocahan S (2023). The roles of long non-coding RNAs in the necroptotic signaling of colon cancer cells. *Mol Biol Rep* 50:5021-5028
- Cai Z, Jitkaew S, Zhao J, Chiang H-C, Choksi S, Liu J, Ward Y, Wu L-g, Liu Z-GJNcb (2014). Plasma membrane translocation of trimerized MLKL protein is required for TNF-induced necroptosis. *Nat Cell Biol* 16:55-65
- Chen CC, Sureshbabul M, Chen HW, Lin YS, Lee JY, Hong QS, Yang YC, Yu SL (2013). Curcumin Suppresses Metastasis via Sp-1, FAK Inhibition, and E-Cadherin Upregulation in Colorectal Cancer. Evidence-based complementary and alternative medicine : eCAM 2013:541695
- Chen T, Yang C, Xi Z, Chen F, Li H (2020). Reduced Caudal Type Homeobox 2 (CDX2) Promoter Methylation Is Associated with Curcumin's Suppressive Effects on Epithelial-Mesenchymal Transition in Colorectal Cancer Cells. *Medical science monitor : International Medical Journal Of Experimental And Clinical Research* 26:e926443
- Cho Y, Challa S, Moquin D, Genga R, Ray TD, Guildford M, Chan FK-MJC (2009). Phosphorylation-driven assembly of the RIP1-RIP3 complex regulates programmed necrosis and virus-induced inflammation. *Cell* 137:1112-1123
- Gong Y, Fan Z, Luo G, Yang C, Huang Q, Fan K, Cheng H, Jin K, Ni Q, Yu XJMc (2019). The role of necroptosis in cancer biology and therapy. *Mol Cancer* 18:1-17
- Guo LD, Chen XJ, Hu YH, Yu ZJ, Wang D, Liu JZ (2013). Curcumin inhibits proliferation and induces apoptosis of human colorectal cancer cells by activating the mitochondria apoptotic pathway. *Phytother Res* 27:422-430
- Guo Y, Shu L, Zhang C, Su Z-Y, Kong A-NTJBp (2015). Curcumin inhibits anchorage-independent growth of HT29 human colon cancer cells by targeting epigenetic restoration of the tumor suppressor gene DLEC1. *Biochem Pharmacol* 94:69-78
- Hanahan D, Weinberg RAJc (2011). Hallmarks of cancer: the next generation. *Cell* 144:646-674
- He S, Wang L, Miao L, Wang T, Du F, Zhao L, Wang XJC (2009). Receptor interacting protein kinase-3 determines cellular necrotic response to TNF- α . *Cell* 137:1100-1111
- Holler N, Zaru R, Micheau O, Thome M, Attinger A, Valitutti S, Bodmer J-L, Schneider P, Seed B, Tschopp JNi (2000). Fas triggers an alternative, caspase-8-independent cell death pathway using the kinase RIP as effector molecule. *Nat Immunol* 1:489-495
- Johnstone RW, Ruefli AA, Lowe SWJC (2002). Apoptosis: a link between cancer genetics and chemotherapy. *Cell* 108:153-164
- Lee YJ, Park KS, Lee SH (2021). Curcumin Targets Both Apoptosis and Necroptosis in Acidity-Tolerant Prostate Carcinoma Cells. *Biomed Res Int* 2021:8859181
- Liu B, Cui LS, Zhou B, Zhang LL, Liu ZH, Zhang L (2019). Monocarbonyl curcumin analog A2 potently inhibits angiogenesis by inducing ROS-dependent endothelial cell death. *Acta Pharmacol Sin* 40:1412-1423
- Marley AR, Nan HJJome, genetics (2016). Epidemiology of colorectal cancer. *Int J Mol Epidemiology Genet* 7:105
- Mosieniak G, Adamowicz M, Alster O, Jaskowiak H, Szczepankiewicz AA, Wilczynski GM, Ciechomska IA, Sikora EJMoa, development (2012). Curcumin induces permanent growth arrest of human colon cancer cells: link between senescence and autophagy. *Mech. Ageing Dev* 133:444-455
- Rana C, Piplani H, Vaish V, Nehru B, Sanyal SN (2015). Downregulation of PI3-K/Akt/PTEN pathway and activation of mitochondrial intrinsic apoptosis by Diclofenac and Curcumin in colon cancer. *Mol Cell Biochem* 402:225-241
- Selvam C, Prabu SL, Jordan BC, Purushothaman Y, Umamaheswari A, Hosseini Zare MS, Thilagavathi R (2019). Molecular mechanisms of curcumin and its analogs in colon cancer prevention and treatment. *Life Sci* 239:117032
- Sun L, Wang H, Wang Z, He S, Chen S, Liao D, Wang L, Yan J, Liu W, Lei XJC (2012). Mixed lineage kinase domain-like protein mediates necrosis signaling downstream of RIP3 kinase. *Cell* 148:213-227
- Sung H, Ferlay J, Siegel RL, Laversanne M, Soerjomataram I, Jemal A, Bray F (2021). Global cancer statistics 2020: GLOBOCAN estimates of incidence and mortality worldwide for 36 cancers in 185 countries. *CA: a cancer journal for clinicians* 71:209-249
- Verma S, Singh SJVw (2008). Current and Future Status of Herbal Medicines 1:347
- Watson JL, Hill R, Yaffe PB, Greenshields A, Walsh M, Lee PW, Giacomantonio CA, Hoskin DW (2010). Curcumin causes superoxide anion production and p53-independent apoptosis in human colon cancer cells. *Cancer Lett* 297:1-8

Bulletin of Biotechnology

Removal of copper (II) from mining waste water by adsorption onto activated carbons produced from hazelnut shell

Pınar Bozbeyoğlu* 

* *Electronics and Automation Department, Gümüşhane Vocational School, Gümüşhane University, Gümüşhane, Turkey*

*Corresponding author : pinarbozbeyoglu@gumushane.edu.tr

Orcid No: <https://orcid.org/0000-0002-3704-2701>

Received : 10/10/2023

Accepted : 08/11/2023

Abstract: Mining wastewater is one of the most important environmental problems today because of the heavy metal ions they contain. Wastewaters containing heavy metal pollution are generally acidic waters with low BOI (Biochemical oxygen demand) value. Various processes such as mineral processing waste disposal, illegal mining, domestic waste disposal, and others result in the release of heavy metals into the waters. One of the heavy metals that cause problems in terms of environmental pollution is copper. Copper metal is commonly found in metal and metal plating industry wastewater. Although metal industry wastewater is low in quantity, they are toxic waste. For this reason, industrial wastewater must be treated before being discharged into the receiving environment. In this study, the amount of Cu in wastewater of the mining operation in Gümüşhane was determined. Heavy metal pollution was eliminated with an adsorbent produced from agricultural biowaste. It has been tried to determine the amount of adsorbent, contact time, and treatment efficiency of wastewater at different pHs of activated carbon produced by chemical activation. As a result, an average of 88.7% efficiency was obtained with activated carbon activated with KOH, while 22.4% copper removal efficiencies were obtained with raw material (hazelnut shell) used without activation. It was determined that the appropriate working pH was 5.0; the amount of adsorbent was 0.05 g and Q_{max} 121.2. As a result, in this study, very low-cost adsorbents were produced using waste hazelnut shells, and a biotechnological approach was proposed to clean copper-containing wastewater.

Keywords: Activated carbon, adsorption, chemical activation, wastewater, hazelnut shell

© All rights reserved.

1 Introduction

Contamination by heavy metals can be in dissolved or suspended forms. The presence of contaminants exceeding permissible limits poses a significant risk of carcinogens in mammals. Copper (Cu) is a metal heavily used in industries such as plating, mining and smelting, brass production, electroplating industries, oil refining and excessive use of Cu-based agricultural chemicals mining (Bozbeyoglu and Doğan 2023). Industries generate wastewater with varying levels of Cu(II) ions, which negatively impact aquatic environments. According to WHO, the exposure limit value of Cu (II) metal in wastewater is 2.0 mg/l. If it exceeds this value, diseases such as kidney failure, allergies and anemia occur in people (Güler et al. 2001; Budak et al. 2022).

The most commonly used techniques for removing Cu(II) ions from wastewater include oxidation, reduction, precipitation, membrane filtration, biological process, ion

exchange, and adsorption. Activated carbons are used in various fields including environmental protection, production of fine chemicals and medicines, food processing, and military activities. Among various purification technologies, activated carbon adsorption is widely used due to its porous surface structure, high surface area, non-harmful nature, and ease of use. However, the high cost of activated carbon has led to the development of new adsorbents with similar properties but lower cost.

The aim of the study was to investigate the performance of Cu(II) adsorption by producing activated carbon from hazelnut shells (HS-AC), which are a type of agricultural biowaste. The use of renewable resources such as biomass is crucial for the sustainable development of the social economy. The study aimed to determine critical factors influencing high surface area activated carbon production from hazelnut shells.

2 Materials and Method

2.1 Materials

Preparation of hazelnut shell and mining waste water

Hazelnuts were collected in Trabzon's farm. Raw hazelnut shells were dried in an oven at 110°C for 12 h to remove the moisture content. The dried shells were smashed up to a size range of 1–2 mm (with a coffee grinder) pulverized physically and sifted through a 60 mesh sieve. A sample of wastewater was collected from the drainage pool in the mining facility. It was transferred to sterile glass bottles and stored at room temperature away from sunlight until analysis.

Preparation of activated carbon

The activated carbon was prepared by following steps: (1) 100 g of the selected fraction of hazelnut shell was impregnated with concentrated KOH. (2) Heated the tube to 750°C at a rate of 30°C/min and kept this condition for 12 h to carbonize the raw material in a hot air oven and then it was washed with distilled water until the pH of the activated carbon reached six, (Fig. 1). (3) The carbonized material was washed with distilled water to remove the free acid. (4) Dried at 105°C, then removed after the furnace cooled to room temperature. The carbonized materials were treated with an activator for 30 minutes (Bansal et al. 2005).



Fig. 1 HS-AC production process

2.2 Characterization techniques

2.2.1 Ash content determination

Ash content of original hazelnut shells (HS) and hazelnut shells activated carbon with KOH (HS-AC) adsorbents was determined using the ASTM (American Society for Testing Materials) standard method. The crucibles were placed inside the muffle furnace and the furnace was set to gradually increase the temperature to 500°C over the course of 1 hour, and then to 750°C over the course of 2 hours. Once the desired temperature was reached, the samples were removed from the furnace and allowed to cool inside a desiccator. Their weight was then measured (El-Hendawy et al. 2001)

2.2.2 Determination of volatile matter amount

The ASTM standard method was employed to determine the volatile matter contents of adsorbents. To prepare for the

experiment, the platinum crucible was first placed in a muffle furnace along with its lid and heated to 950°C for 30 minutes. After that, 1 gram samples were added to the crucibles, and the crucibles with their contents were kept in the muffle furnace at 950°C for a further 10 minutes. The samples were removed from the oven, cooled in a desiccator and weighed.

2.2.3 Boehm Titration

With Boehm titration, surface functional groups of various adsorbents and especially activated carbons can be detected (Boehm 1966). To quantify the number of lactonic, phenolic, and carboxylic groups in mmol for both adsorbents through Boehm titration, 0.05g of adsorbent was treated with 50mL of 0.1N NaOH, NaHCO₃, and Na₂CO₃ separately. The mixture was then shaken at 400rpm for 24 hours. Total surface acidic groups (lactonic, phenolic, and carboxylic) were all neutralized with 0.1 N NaOH and determined. After shaking and filtration, the filtrate was titrated with 0.1 N HCl (Duman et al. 2009).

2.2.4 pH and pH at neutral load point (pHpzc)

0.1 g of adsorbent was mixed with a 0.1 M NaCl solution. The mixture was shaken for 24 hours at pH values ranging from 2 to 10 to determine pHpzc values of the adsorbent. As a result of shaking, the adsorbent and the solution were separated from each other by centrifugation, and the equilibrium pH values of the solutions were measured with a pH meter. The point where the graph cuts the x-axis from the y-zero value is recorded as pHpzc (Duran et al. 2011).

2.2.5 FT-IR analysis

Thoroughly dried adsorbent samples (few mg) were measured before and after adsorption using direct spectra in the FT-IR device within the 200-4000 cm⁻¹ wavelength range.

2.3 Equilibrium, kinetic and thermodynamic parameter

For the characterization of HS and HS-AC the effects of pH, contact time, temperature, and amount of adsorbate-adsorbent as adsorption tests from aqueous solution were investigated in conjunction with equilibrium, kinetic, and thermodynamic parameters (Bozbeyoglu et al. 2020).

2.4 Adsorption tests

Optimum pH values were determined on activated carbons. pH values of metal-containing mining wastewater were adjusted to pH 5.0 for Cu. Then, 10 mL of each of these solutions (5.0 g/L activated carbon suspension), whose pH was adjusted, were treated separately with 0.05 g of activated carbons for 6 hours. After the completion of the process, the metal concentrations in the solutions filtered with a 0.45 μm nitrocellulose membrane through a vacuum filtration device were determined using MP-AES. Each trial was performed in at least three parallels, and the averages of the results were given. 1g with the help of the remaining adsorbate concentration (*C_e*) without being adsorbed in the solution (Gündoğdu 2010; Bozbeyoglu 2020).

The amount of adsorbate adsorbed by 1 g of adsorbent is calculated in mg/g with the following formula:

$$Q_e = \frac{(C_o - C_e) \cdot V}{m}$$

Percent adsorption was also calculated with the following formula:

$$\text{Adsorption}(\%) = \frac{C_o - C_e}{C_o} \cdot 100$$

Q_e : The amount of adsorbate adsorbed by 1 g of adsorbent (mg/g)

C_o : Initial adsorbate concentration (mg/L)

C_e : The amount of adsorbate remaining without being adsorbed in solution at equilibrium (mg/L)

V : Adsorbate volume (mL)

m : Amount of adsorbent (g)

MA : Atomic or molar mass (g/mol)

3 Results

3.1 Characterization Analysis Results

Moisture, volatile matter, fixed carbon and ash content results

The results obtained regarding moisture, ash, volatile matter, fixed carbon analyses, and production yields of this HS-AC and original HS are given in Table 1. High moisture adsorption of activated carbons is normally undesirable. The activated carbon produced has a higher moisture content compared to the starting material HS. It is expected that H₂O molecules are trapped inside the pores of HS-AC, due to its more porous structure compared to HS. When examining the volatile matter content of adsorbents, HS, the starting material, has the highest amount of volatile matter, as expected. Since no heat treatment is used, HS contains high levels of volatile organic compounds.

Table 1. Brief analysis results of adsorbents

Parameters (%)					
Sample	Moisture	Volatile matter	Fixed carbon	Ash	yield
HS	4.7	79.2	11.9	4.2	-
HS-AC	15.1	21.7	53.0	10.2	75.3

Elemental Analysis Results

Table 2 shows the results of the elemental analyses performed on the adsorbents using the Leco CHNS 932 elemental analyzer. The oxygen amounts presented in the table are calculated based on the difference. The analysis revealed that the fixed carbon amounts of the produced activated carbon are higher than those of the HS-AC (Akyıldız 2007). During the production of activated carbon, hydrogen, and oxygen are separated from the structure along with volatile components in the gas phase.

Table 2. Element Contents of Adsorbents (%)

Element Contents (%)						
Sample	C	H	N	S	*O	**C/H
HS	47.6	6.23	0.87	0.14	49.70	7.64
HS-AC	58.53	2.96	0.28	-	38.23	19.77

*Calculated from difference. **Mole ratios-Not determined

Determination of pH and pH_{pzc}

Figure 2. shows the graph of equilibrium pH values versus initial pH of adsorbents. It is observed that the initial pH values slightly change after 24 hours of treatment in the unbuffered system. In other words, since the buffer system is not used when adjusting the initial pH, the surface functional groups of the adsorbents can easily interact with the H⁺ and OH⁻ ions in the solution.

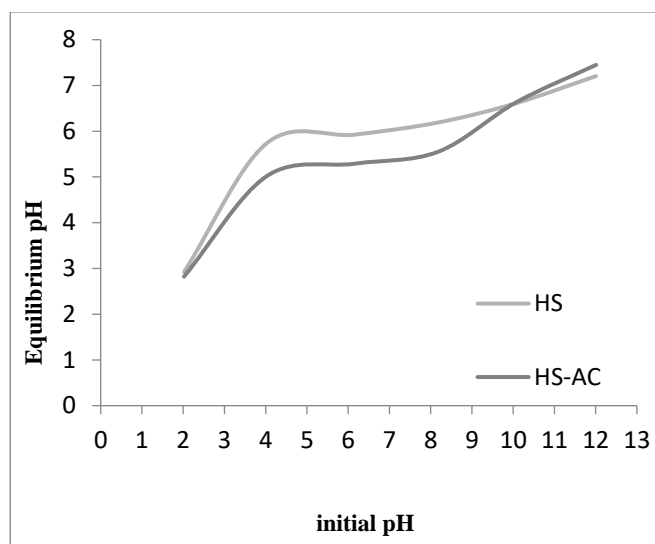


Fig. 2 Initial pH vs. equilibrium pH plot for pH_{pzc} determination (variation between initial pH and equilibrium pH)

Scanning electron microscopy (SEM) analysis

The surface of the adsorbent was characterized by scanning electron microscopy (SEM, Philips XL30S-FEG). It interacted with the hazelnut shell in chemical activation, as seen from the porosity after treatment with potassium hydroxide (Condon 2006). Although the porosity is homogeneous, deep enough pores are not formed, resulting in low surface area. HS-AC has a significant number of pores that trap and adsorb metal ions (Fig. 3).

The fact that the pore walls are thicker than other activated carbons can be explained by the reaction of potassium with the organic structure. Pore width (nm) for HS and HS-AC was measured by BET (Brunauer–Emmett–Teller nitrogen adsorption technique) (Fig. 4)

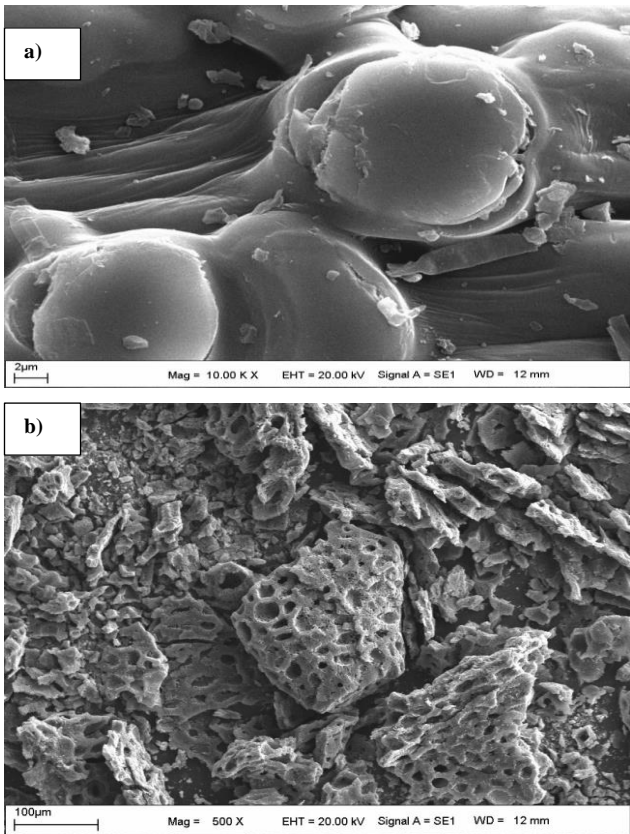


Fig. 3 SEM images for (a) HS and for (b) HS-AC

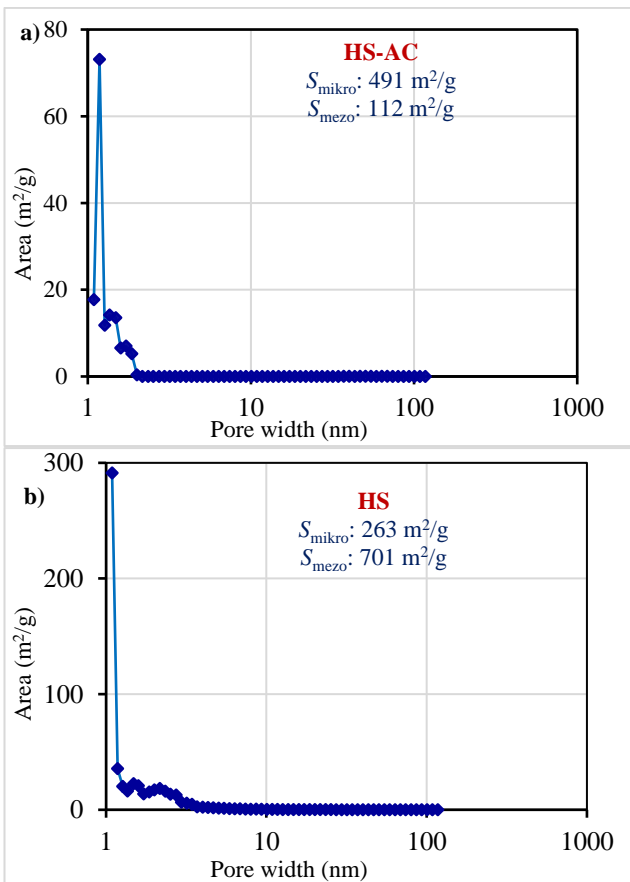


Fig. 4 Pore width (nm) for (a) HS-AC and for (b) HS

Boehm titration

The results from the Boehm titrations for determining surface functional groups are presented in Table 3. As can be seen from the table, the produced activated carbon has rich acidic groups on its surface.

Table 3. Quantitative amounts of surface acidic groups by Boehm Titration for adsorbents

Adsorbent	Acidic groups (mmol/g)			
	Total acidic groups	Carboxylic groups	Phenolic groups	lactonic groups
HS	2.63	1.90	0.41	0.32
HS-AC	6.30	1.74	3.24	1.32

Iodine and methylene blue numbers

The iodine number measures microporosity, referring to 0-2 nm pores. A relatively high iodine number also indicates that the relevant adsorbent has a high surface area (especially high microporosity) (Döşemen 2009). The methylene blue number is a measure of the ability of the adsorbent to adsorb larger organic molecules. Increasing surface area, porosity, and active groups enhance iodine and MB adsorption (Sun 2010). Figure 5 gives a comparison of iodine numbers and MB numbers of adsorbents.

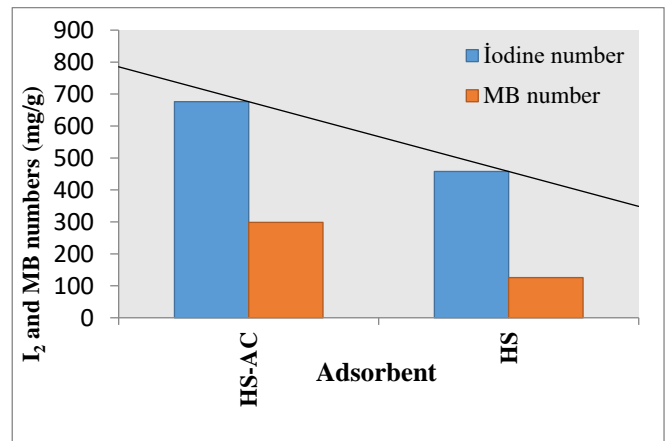


Fig. 5 Comparison of I₂ and MB numbers of adsorbents

FTIR and XRD analysis results

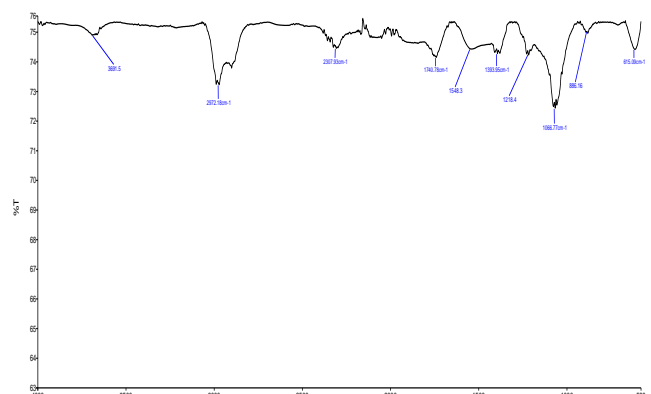


Fig. 6 IR Spectrum for HS-AC

When the IR spectrum for HS-AC is examined in Figure 6; The slightly broad peak appearing at 3691cm^{-1} is due to the moisture and/or hydroxyl ($-\text{OH}$) groups contained in the sample. Hydroxyl containing groups; phenols, alcohols and carboxylic structures. It is expected that these groups already exist within the original Central Committee, but they undergo deformation at high temperatures during activated carbon production, except for HS-AC (Fig. 6). The peaks appearing at 2972 and 2307cm^{-1} belong to aliphatic C-H bonds. The peak appearing at 1740cm^{-1} is the carbonyl (C=O) stretching peak.

XRD and BET anaysis results

As can be seen from Fig. 7, the major peak associated with Na at $2\theta = 25^\circ$ for hazelnut shell ash, also peaks of Ca, K, P, KCl, CaCl_2 , KCl are found according to the library data of the XRD instrument. The hazelnut shell ash primarily consists of silica. XRD pattern shows amorphous silica structure at $2\theta = 20^\circ$. All the carbon samples have two broaden peaks around $2\theta = 22^\circ$ and $2\theta = 46^\circ$ which indicates (002) and (001) planes of graphitic structure. These peaks are characteristics of amorphous carbon with a turbostratic structure. This means that graphite-like microcrystallites are bounded by a crosslinking network of several graphite-like layers, with each layer having a random direction. Furthermore, it is worth noting that low intensity and wide peaks indicate that some graphite-like amorphous structures have been formed and the sharp and narrow peaks show that highly ordered graphite-like structures.

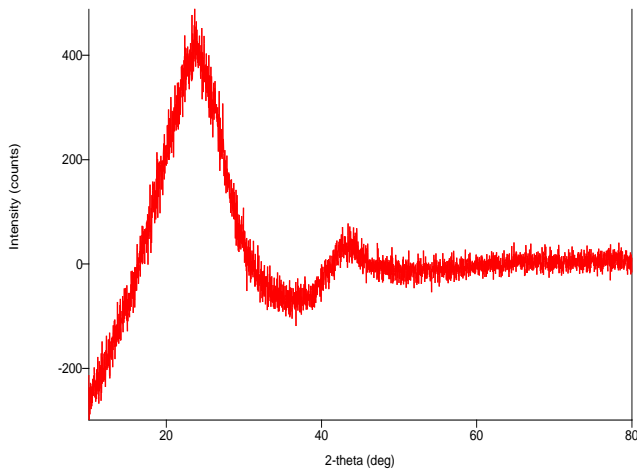


Fig. 7 XRD Spectrum for HS-AC

Table 4. BET surface areas and pore size distributions of adsorbents

Ads	S_{BET} m^2/g	S_{mikro}		S_{mezo}		V_{toplam} cm^3/g	V_{mikro}		V_{mezo}		D_p^a nm
		m^2/g	%	m^2/g	%		cm^3/g	%	cm^3/g	%	
HS	0.12	0.12	100	-	-	0.003	0.03	100	-	-	-
HS-AC	598.6	-	-	-	-	0.32	0.27	83.6	0.05	16.4	2.12

S_{BET} : BET surface area *S_{mikro}*: Micropore surface area
S_{mezo}: Mesopore surface area *V_{total}*: Total *D_p* : Average pore diameter
 - : Could not be determined

HS has a mostly microporous structure, while HS-AC is more mesoporous.

3.2 Adsorption analysis results and equilibrium, kinetic and thermodynamic parameters

3.2.1 Effect of initial Cu(II) concentration and adsorption isotherms

Adsorption of Cu (II) from aqueous solution on the adsorbent fixed amount to investigate the effect of the initial Cu(II) concentration. A serial Cu solution in the range of adsorbent (1.0 g/L) and 50–1000 mg/L under optimum conditions was treated. The C_e-Q_e graph drawn in the light of the data shows that a rapid increase in adsorption at the beginning that the increase slows down and progresses towards reaching equilibrium (Fig. 8). In this study, the Langmuir and Freundlich isotherm models were used to analyze the results.

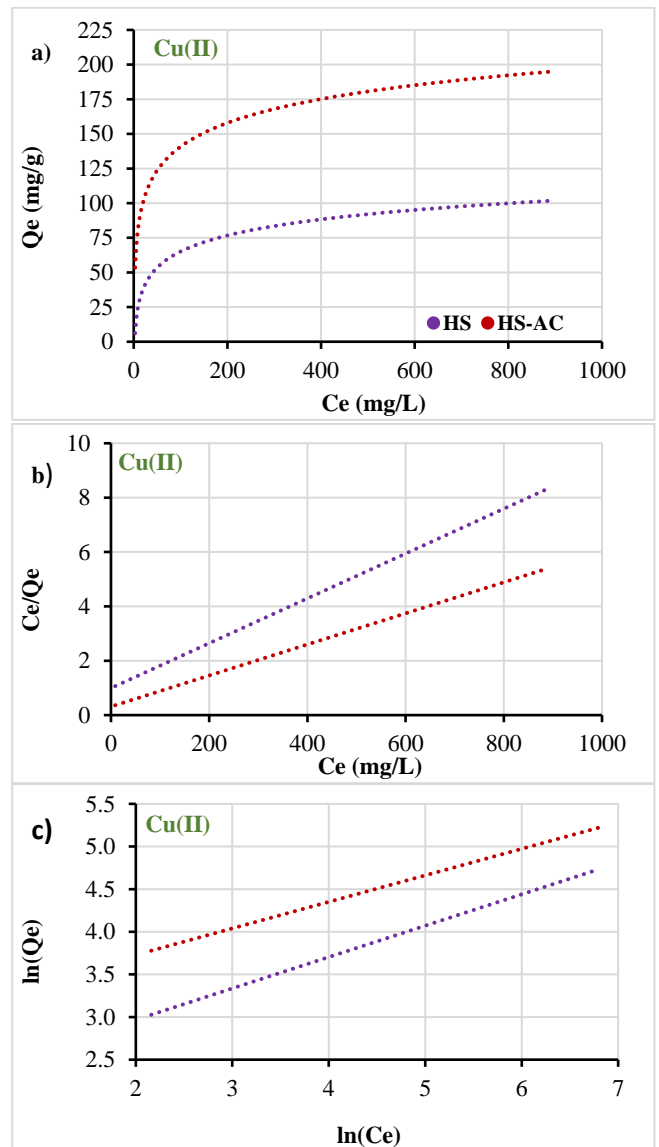


Fig. 8 Effect of initial Cu(II) concentration and adsorption isotherms: (a) C_e vs Q_e graphs, (b) C_e vs C_e/Q_e graph for Langmuir isotherm (c) $\text{Ln}(C_e)$ vs $\text{Ln}(Q_e)$ for Freundlich isotherm, graph for Cu(II) adsorption on HS-AC (Initial Metal conc: 50–1000 mg/L, pH: 5.0, HS-AC dose: 1.0 g/L)

This theoretical equilibrium isotherm, developed by Langmuir, accepts that there are receptor points on the surface of the adsorbent and that each receptor point can adsorb only one molecule, so the resulting layer will be one molecule thick.

$$\frac{C_e}{Q_e} = \frac{C_e}{Q_{maks}} + \frac{1}{bQ_{maks}}$$

Q_e: Amount of adsorbate adsorbed by 1 g of adsorbent (mg/g)

Q_{max} : Maximum monolayer adsorption capacity (mg/g)

C_e: The amount of adsorbate remaining unadsorbed in the solution at equilibrium (mg/L)

b: Constant related to free energy or adsorption enthalpy (L/mg)

It is often observed that the Freundlich isotherm is followed in situations where there is multilayer adsorption. The equation of the model expressing the change of the amount of substance (*Q_e*) adsorbed by the adsorbent with pressure and concentration is expressed below (Freundlich 1906);

$$Q_e = K_f \times C_e^{1/n}$$

Table 5. Langmuir and Freundlich isotherm constants obtained for Cu (II) adsorption

Cu (II)	Langmuir constants				Freundlich constants		
	Q _{maks} (mg/g)	Q _{maks} (mmol/g)	b (L mg ⁻¹)	R ²	K _f (mg g ⁻¹)	n	R ²
HS	54.4	1.80	0.0129	0.9879	17.54	3.72	0.9979
HS-AC	121.2	1.91	0.0346	0.9984	30.96	4.81	0.9667

The Langmuir and Freundlich adsorption equations were used to expiries adsorption phenomenon of the Cu (II). The Freundlich (R²: 0,9979) isotherm model at those optimum conditions best defined the equilibrium data of HS but for the HS-AC is suitable for the Langmuir isotherm model (R²:0,9984)

3.2.2 Effect of temperature on adsorption of Cu(II) on activated carbon and adsorption thermodynamics

Q_e graphs drawn against the studied temperature values are given in Fig. 6. As can be seen, the adsorption behavior of Cu ions on the relevant adsorbents proceeds through an endothermic mechanism. To put it simply, the adsorption efficiency is enhanced by higher ambient temperatures. Additionally, the thermodynamic constants of adsorption were assessed. The negative value of ΔG° confirms the spontaneous nature of the adsorption process. The positive value of ΔS° shows that the randomness at the solid solution interface increases during adsorption, while the positive value of ΔH° indicates that the adsorption process is endothermic.

Table 6. Thermodynamic data for Cu(II)

Thermodynamic data for Cu(II)					
Adsorbent	T (°C)	K _d	ΔG° (kJ/mol)	ΔS° (J/mol.K)	ΔH° (kJ/mol)
HS	5	0.66	0,96	22.37	7.11
	15	0.77	0,63		
	25	0.85	0,41		
	35	0.94	0,16		
	50	1.01	-0,03		
HS-AC	5	1.82	-1,38	32.77	7.67
	15	2.10	-1,78		
	25	2.41	-2,18		
	35	2.59	-2,44		
	50	2.89	-2,85		

The effect of temperature Cu (II) uptake capacity onto HS-AC was studied at 100 mg/L initial metal ion concentration.. Adsorption studies were carried out for 24h and it was observed that, the amount of adsorbed Cu (II) increased linearly with time at the beginning of adsorption. A larger amount of Cu (II) ions was removed in the first 10 min of contact time and the equilibrium was established in 30-60 min at the end of a rapid adsorption for all temperatures studied. After a period of 120 minutes, the adsorption of Cu (II) reached equilibrium and there was no further adsorption. The optimal temperature for Cu (II) adsorption was found to be 60°C. Removal of copper (II) ions increased with temperature up to 60°C.

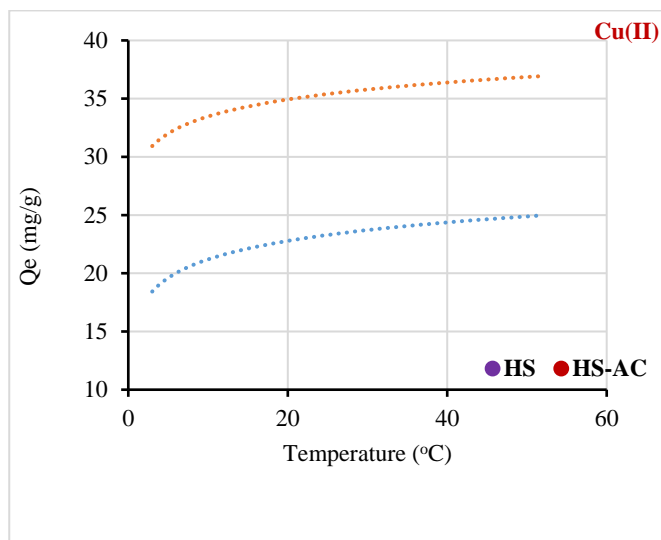


Fig. 9 Effect of Temperature: Temp. vs Q_e graph and (Initial Cu conc.: 250 mg/L, pH: 5.0, HS-AC dose: 5.0 g/L)

3.2.3 Effect of contact time and adsorption kinetics on the adsorption of Cu(II) ions on activated carbons

Adsorbents in amounts of 5.0 g/L were treated with solutions with pH values of 5.0 for Cu (II) ions, for periods of 0–12 hours. The solutions collected at specific intervals using a micropipette were determined via MP-AES, and the remaining amounts were calculated. Here, the amount of metal loaded per gram of adsorbent was calculated (mg/g). Qt graphs drawn from the obtained data against time are shown in Fig. 10. From the figure, it is evident that the time required to attain equilibrium for all metal ions is quite short, and the process is completed in almost two hours. However, to ensure complete balance for all metal ions, it was decided to extend the processing time to four hours (Mafra 2013).

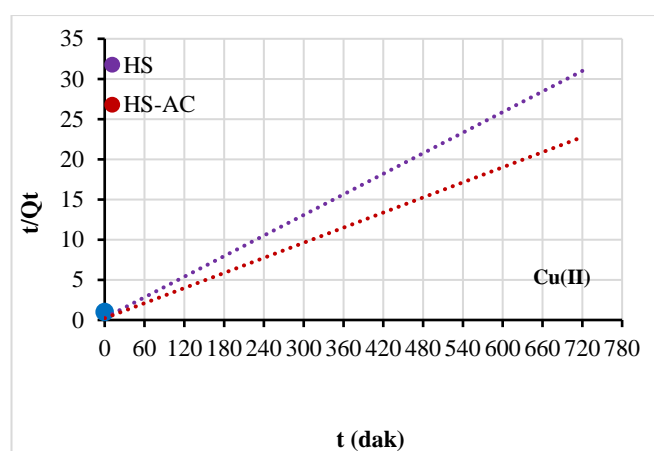


Fig. 10 Effect of contact time and kinetics on adsorption of Cu by HS-AC (Initial pH: 5.0, initial Cu concentration: 250 mg/L, HS-AC dose: 5.0 g/L, agitation time: 12 h)

Various kinetic models namely the Lagergren's pseudo-first order, pseudo-second order, and intraparticle diffusion models have been used for the validity of the experimental adsorption process for Cu (II) onto HS-AC. The HS-AC can be used as an effective low-cost agricultural waste adsorbent for the removal of Cu (II) with HS-AC's adsorption capacity Q_{Max} : 121.2 mg/g at 60°C. The kinetics of Cu (II) adsorption onto HS-AC was examined using the pseudo-first and pseudo-second order kinetic models. The results indicated that the Intraparticle diffusion equation provided the best correlation of the sorption data. The values of various kinetic parameters are tabulated in Table 7. The results showed that, the correlation coefficient for the Intraparticle diffusion model obtained 20–60°C was very low and they increased with increasing temperature.

The pH of an aqueous solution is an important controlling parameter in the process of adsorption. The adsorption capacity of copper (II) ions by HS-AC was analyzed in a pH range of 2–12. The study found that removal of copper (II) ions increased as solution pH increased, and reached a maximum at an equilibrium pH of about 4 when the initial copper (II) ion concentration was 100 mg/L. Experiments were carried out up to pH value of 5 due to the fact that metal precipitation occurred at higher pH values. At very low pH values (pH=2–3), copper (II) ion adsorption was found to be very low due to competition between H_3O^+ and

copper (II) ions for the adsorption sites. In addition when the pH increases, there is a decrease in positive surface charge, which results in a lower electrostatic repulsion between the positively charged metal ion and the surface of HS-AC, favoring adsorption. The study revealed that the loading of copper (II) ions onto HS-AC increased until pH 4 and then remained constant until pH 5. Beyond pH 6, hydroxide precipitations occurred. These precipitations, along with adsorption, contributed to the removal of metal ions.

Table 7. Kinetic data for adsorption of Cu(II) ions from wastewater on HS-AC

	Constants	HS	HS-AC
Cu(II)	Q_e (den), mg/g	23.20	31.60
Pseudo 1st order kinetics	k_1 , dak^{-1}	8.17	11.33
	R^2	0.01185	0.01151
	Q_e (hes), mg/g	0.8885	0.8505
Pseudo 2nd order kinetics	Q_e (hes), mg/g	23.42	31.93
	R^2	0.00688	0.00448
	K_{id} , $mg/g.dak^{1/2}$	16.39	20.11
Intraparticle diffusion	C , mg/g	0.577	1.042
	R^2	0.9998	0.9998
	k_1 , dak^{-1}	0.7655	0.8135

3.2.4 Effect of pH on the adsorption of Cu(II) ions on activated carbons

4 Discussion

By examining the performance of activated carbon produced by potassium hydroxide activation, it has been determined in studies that hazelnut shell wastes thrown into the environment, can be used as an adsorption material. Thus, a biotechnological approach was created by cleaning the wastewater of mining enterprises that pollute the environment with another waste. In our study, the optimum pH range for Cu metals determined to be around 5, the amount of adsorbent decreased, the agitation time increased, the adsorption capacity increased. The results showed that, the correlation coefficient for the Intraparticle diffusion kinetic model obtained 20–60°C was very low and they increased with increasing temperature. It is seen that the Freundlich isotherm model is more suitable for the adsorption of metals on HS, and the Langmuir isotherm model for Cu (II) adsorption on HS-AC. These results showed that activated carbon can be produced from hazelnut shells by chemical activation with KOH, and that this method is a cost-effective and energy-saving method and can help produce activated carbon in a cleaner and greener way.

5 Conclusion

Since hazelnut shells, which are completely agricultural biowaste, were used as material in this study, activated carbon, which was consumed and imported in Turkey, was produced and a local and natural adsorbent was synthesized. This process will significantly decrease the production cost, which is currently the biggest obstacle to the widespread use of activated carbon. Furthermore, it will enable large-scale production of activated carbons using agricultural biowastes and pave the way for their use in various agricultural and daily-life applications.

Acknowledgements



This research did not receive any specific grant from funding agencies in the public, commercial, or not-for-profit sectors.

References

- Akyıldız H (2007) H₃PO₄ aktivasyonu ile zeytin çekirdeğinden aktif karbon üretimi. Yüksek lisans tezi İstanbul Teknik Üniversitesi s. 88s
- Bansal RC, Goyal M (2005) Activated carbon adsorption. CRC press s. 46-48
- Bozbeyoğlu P (2020) Karadeniz bölgesinde yetişen mısırların koçanından aktif karbon üretimi, karakterizasyonu ve atık sulardan çeşitli kirleticilerin uzaklaştırılmasında kullanımının incelenmesi. Doktora Tezi Gümüşhane Üniversitesi s.68
- Bozbeyoğlu P, Duran C, Baltacı C, Gundogdu A (2020) Adsorption of methylene blue from aqueous solution with sulfuric acid activated corn cobs: equilibrium, kinetics and thermodynamics assessment. Hittite J Sci Eng 7(3):239–56
- Bozbeyoğlu P, Doğan O (2023) Determination of chemical risk factors in chemical laboratories. Current Research in Science and Mathematics ISBN:978-625-430-716-4, s.104-119
- Budak B, Dinçkaya E (2022) L-Askorbik asit (Cvitamini) tayinine yönelik kalem grafit elektrot-askorbat oksidaz temelli yeni bir biyosensör geliştirilmesi. Int J Life Sci Biotechnol 5(3):611-626
- Condon JB (2006) Surface area and porosity determinations by physisorption. Measurements and Theory 147(11):578-584
- Döşemen Y (2009) Kestane Kabuğundan Aktif Karbon Üretimi. Yüksek lisans tezi İstanbul Teknik Üniversitesi s. 89
- Duman G, Önal Y, Okutucu C, Önenç S, Yanık, J (2009) Production of activated carbon from pinecone and evaluation of its physical, chemical, and adsorption properties. Energy & Fuels 23(20):2197–2204
- Duran C, Özdeş D, Gündoğdu A, İmamoğlu M, Şentürk HB (2011) Tea industry waste activated carbon, as a novel adsorbent, for separation, preconcentration and speciation of chromium. Anal Chim Acta 688(1):75-83
- El-Hendawy AN, Samra SE and Girgis BS (2001) Adsorption characteristics of activated carbons obtained from corncobs, colloids and surfaces. Physicochem Eng Asp 180(3):209-221
- Freundlich HF (1906) Über die adsorption in lösungen. Z fur Phys Chem 57:385-470
- Güler Ç, Çobanoğlu Z (2001) Su kirliliğinin. TC. Sağlık Bakanlığı Çevre Sağlığı Temel Kaynak Dizisi No:12, Ankara, s.64
- Gündoğdu A (2010) Fabrika çay atıklarından aktif karbon üretimi, karakterizasyonu ve adsorpsiyon özelliklerinin incelenmesi. Doktora Tezi Karadeniz Teknik Üniversitesi s. 72

Bulletin of Biotechnology

Investigation of the antioxidant and antibacterial effects of fermented *Cornus mas* and *Rubus sanctus* fruits

Derya Ünal¹ , Tuba Sevimoğlu^{2*} 

¹Department of Bioengineering, Üsküdar University, İstanbul, Türkiye

²Department of Bioengineering, University of Health Sciences, İstanbul, Türkiye

*Corresponding author : tuba.sevimoglu@sbu.edu.tr

Orcid No: <https://orcid.org/0000-0003-4563-3154>

Received : 11/10/2023

Accepted : 10/12/2023

Abstract: In this study antioxidant and antibacterial activities of fermented *Cornus mas* and *Rubus sanctus* berries collected from province of Bartın in the Western Black Sea region of Türkiye were analyzed. Prior to fermentation with *S. cerevisiae*, the fruits were tested for 58 pesticides such as Dicloran and Quintozene and none of the pesticides were detected. The presence of ascorbic acid in the fruits, which is a nutrient needed by the body, was also detected by FTIR. Then the pesticide free berries were crushed, and the samples were fermented separately. Testing after the fermentation process revealed the samples contained ethyl alcohol. Antioxidant activities of fermented samples were analyzed using CUPRAC, DPPH and Folin Ciocalteu methods. The results suggest high antioxidant contents of the fermented samples. Evaluation of antimicrobial activity was done through disk diffusion method using *P. aeruginosa* and *S. aureus* suggesting that these samples do not suppress these bacteria for the studied concentrations. Furthermore, the growth of *C. albicans* was examined immediately, demonstrating that the fermented samples do not show antifungal effects. The reason for these shortcomings could be inadequate concentration levels. The antioxidant content of these fermented fruits is intended to contribute to human health.

Keywords: *Cornus mas*; *Rubus sanctus*; Fermentation; Antioxidant; Antibacterial

© All rights reserved.

1 Introduction

Throughout life human beings are continuously exposed to factors like radiation, water pollution, environmental pollution, and pesticides etc... As a result of these exposures, free radicals emerge. Free radicals circulate throughout the body to pair their electrons. During this circulation, they cause damage to the body weakening the immune system. Ascorbic acids, thiols, and polyphenols are examples of antioxidants that provide their own electrons to the body's defense against free radical production (Lobo et al. 2010). Fruits and vegetables contain secondary metabolites called phenolic compounds, which have antibacterial properties and inhibit the growth of bacteria, yeast, and viruses (Soong et al. 2019).

Fermented foods provide many health benefits such as antioxidant, antimicrobial, antifungal, anti-inflammatory, anti-diabetic and anti-atherosclerotic activity (Şanlıer et al. 2019).

In this study antioxidant and antibacterial effects of fermented samples of *C. mas* and *R. sanctus* fruit extracts were analyzed. In addition, tests were done to check for pesticides and ascorbic acid content before fermentation and ethyl alcohol formation after fermentation.

2 Materials and Method

2.1 Obtaining *Cornus mas* and *Rubus sanctus* Fruits

C. mas and *R. sanctus* fruits grown in the province of Bartın in the Western Black Sea region of Türkiye were collected ripe in July and August. Fruits were stored in sterilized bags at -20°C.

2.2 Determination of Pesticides

Frozen *C. mas* and *R. sanctus* were thawed. At the end of the dissolution period, the fruits were ground using a metal grinder and pre-treatments were applied respectively according to the pesticide analysis protocol. Each pureed fruit sample was diluted and injected into the GC-MS system separately and the analysis results were recorded.

2.3 Detection of the Presence of Ascorbic Acid

The pureed fruits were compared with the Ascorbic acid CRS standard with the Agilent Cary 630 FTIR spectrometer. Ascorbic acid is defined in the library of the CRS standard devices. Measurements and comparisons were done after the samples were poured over the device's "crystal" section.

2.4 Fermentation

After the frozen fruits were brought to room temperature, they were ground in a grinder and mashed for fermentation. Approximately 20 mg of *C. mas* and *R. sanctus* pureed samples were weighed and taken into four different flasks. *S. cerevisiae*, which was used as the fermenting agent, was added to each sample. 20 ml and 40 ml ultrapure water was added to separate flasks. The samples were sealed, and the fermentation continued for one week. To check for ethyl alcohol presence, the fermented samples were prepared in accordance with the gas chromatography protocol. The prepared samples were injected into the GC-FID device with the ethyl alcohol standard. The results were calculated with the help of the Empower program.

2.5 Antifungal Activity Analysis

SDA (Sabouraud Dextrose Agar) medium was prepared and poured into 12 petri dishes (Two concentrations for each fruit extract done in triplicate) and set for 15 minutes to dry. *C. albicans* (ATCC 10231), which is a common fungus, was selected for the analysis. To prepare a suspension from the *C. albicans* strain, it was immersed in the solution in the glass tube with a sterile swab under the biosafety cabinet. Then, the *C. albicans* suspension was dipped into petri dishes. Microorganism suspension was applied to the entire surface of the agar on the petri dishes with a sterile cotton swab. The petri dishes were set aside for 15 minutes to dry. Fermented samples were spread one by one on the dried agars with sterile cotton swabs. Petri dishes were incubated at 20-25 °C and observed for five days (Collins 2004).

2.6 Antibacterial Effect Analysis

Fermented samples were studied on *S.aureus* (ATCC 6538) and *P.aeruginosa* (ATCC 9027) bacteria to check for their antibacterial activity (Bayer et al. 1966). Firstly, the bacteria, which were stored as colonies, were taken from the media with a swab with disposable plastic extracts and dissolved in the glass tube in the purchased solution to dissolve the bacteria. The prepared frozen TSA (Tryptic Soy Agar) medium was then dissolved in the ultrasonic bath. The medium, whose dissolution was completed, was poured into 12 petri dishes, and waited for drying. The bacteria-containing solution in the glass tube was applied to the drying media with the help of a sterile cotton swab. The petri dishes were incubated at 20-25°C for 24 hours. At the end of the incubation period, 8 mm wells were opened in the medium and 50 µl samples were inoculated into the wells with a micropipette. The samples were incubated at 35-37°C for 24 hours and the results were evaluated.

2.7 Antioxidant Activity Analysis

Fermented samples were prepared in accordance with the protocols of CUPRAC, DPPH and Folin Ciocalteu

antioxidant capacity analysis methods. The prepared samples were read in the UV-VIS device at wavelengths suitable for the analysis methods and calculated.

2.7.1 CUPRAC Assay

The method developed by Apak et al. was used (Apak et al. 2007). This capacity analysis method named "Copper (II) Reducing Antioxidant Capacity (CUPRAC) involves reduction of the copper-neocuproin complex $[Cu(Nc)_2]^{2+}$ by antioxidant in the presence of ammonium acetate to form the copper-neocuproin complex $[Cu(Nc)_2]^{+}$. It is a yellow-coloured compound with maximum absorbance at 450 nm. First ammonium acetate buffer is prepared. 19.3 grams of ammonium acetate reagent was transferred to a 250 ml flask and made up to volume with distilled water. Then, 0.01 M copper (II) chloride solution was prepared by weighing 0.43 gr $CuCl_2 \cdot 2H_2O$ and made up to 250 ml with distilled water. Lastly, 0.0075 M Neocuproin (2,9-dimethyl 1.10 phenanthroline) solution was prepared by weighing 0.16 grams and making up to 100 ml with ethanol. Gallic acid was used as standard. The samples were prepared in 3 different concentrations by adding 20µl, 40µl and 60µl from the sample solution. The solutions were kept in a dark area for 30 minutes at room conditions. The blank, standards and samples prepared according to the procedure were read by zeroing against the blank at 450 nm and the results were recorded.

2.7.2 Folin Ciocalteu Assay

Fruits and vegetables contain phenolic compounds. They can be oxidized in a basic environment, react with a yellow solution hue, and eventually turn blue. The reason for the formation of this color is that the Folin Ciocalteu reagent is kept in a basic environment. Phenolic substances are measured spectrophotometrically at 700–760 nm with the observation of color change (Lussignoli et al. 1999). Fermented *C. mas* and *R. sanctus* samples with two different concentrations (1 mg/ml and 0.5 mg/ml) were diluted 1/10 with methanol. Samples were vortexed for 30 seconds. Gallic acid was used as standard. 0.5 N Folin reagent was prepared by taking 25 ml of 2 N Folin Reagent from the stock bottle and completing it to 100 ml with distilled water. For 10% Na_2CO_3 solution, 1 gram of Na_2CO_3 was weighed to 10 ml, made up to volume with distilled water and mixed. Then, 16 glass tubes were named and put into a tube holder one by one. Blank, standards and samples were prepared with a final volume of 3 ml, respectively.

2.7.3 DPPH Assay

The main feature of the DPPH (2,2-Diphenyl-1-picrylhydrazyl) method is that the transfer of positive charge from the antioxidant substance to the DPPH free radical causes a decrease in absorbance at 517 nm (Sanchez-Moreno et al. 1999). For 0.1 M DPPH radical solution, 39.5 mg of DPPH reagent was weighed and made up to 100 ml with ethanol. The samples were diluted 1/10 with methanol. The blank and samples were prepared by taking 200 µL, 400 µL and 600 µL from the fermented samples, respectively. The prepared solutions were kept in the dark for 30 minutes and read at a wavelength of 517 nm in a spectrophotometer, zeroed against the blank.

3 Results

3.1 Pre-fermentation Analysis

Pesticide and ascorbic acid analysis were done prior to the fermentation process. 58 pesticides (Table 1) were analysed in the GC-MS device. No pesticide residues were detected in the analysed samples. In the analysis of the presence of ascorbic acid with the FTIR-IR device, the presence of ascorbic acid was determined from the similarity between the wavelengths of 2000-1000 in the chromatograms obtained because of the analysis (Fig 1).

Table 1 Pesticides analysed using GC-MS

Biphenyl	Delta-HCH	Bromophos-methyl	Quintozene
THPI	Chlorthalonil	Chozolinate	Tefluthrin
Tecnazene	Formothion	Heptachlor exoepoxide	4,4-DDE
Diphenylamine	Ethofumasate 2-Keto	Heptachlor endoepoxide	Dieldrin
Ethalfuralin	Parathion-methyl	Captan	Oxyfluorfen
Trifluralin	Chloropyrifos-methyl	Folpet	2,4-DDD
Alpha-HCH	Vinclozolin	Procymidone	Chlorfenapyr
Hexachlorobenzene	Heptachlor	Chlordane trans	Endrin
Dicloran	Fenitrothion	Chlordane cis	Dicofol
Beta-HCH	Ethofumasate	Bromophos-ethyl	Chlorthal dimethyl
Gamma-HCH	Aldrin	2,4-DDE	Chlorobenzilate
Beta endosulfan	2,4-DDT	Alpha endosulfan	4,4-DDT
4,4-DDD	Tetrasul	Chlorfenson	Iprodione
Bromopropylate	Tetradifon	Quinoxifen	Cyhalothrin
Methoxychlor			

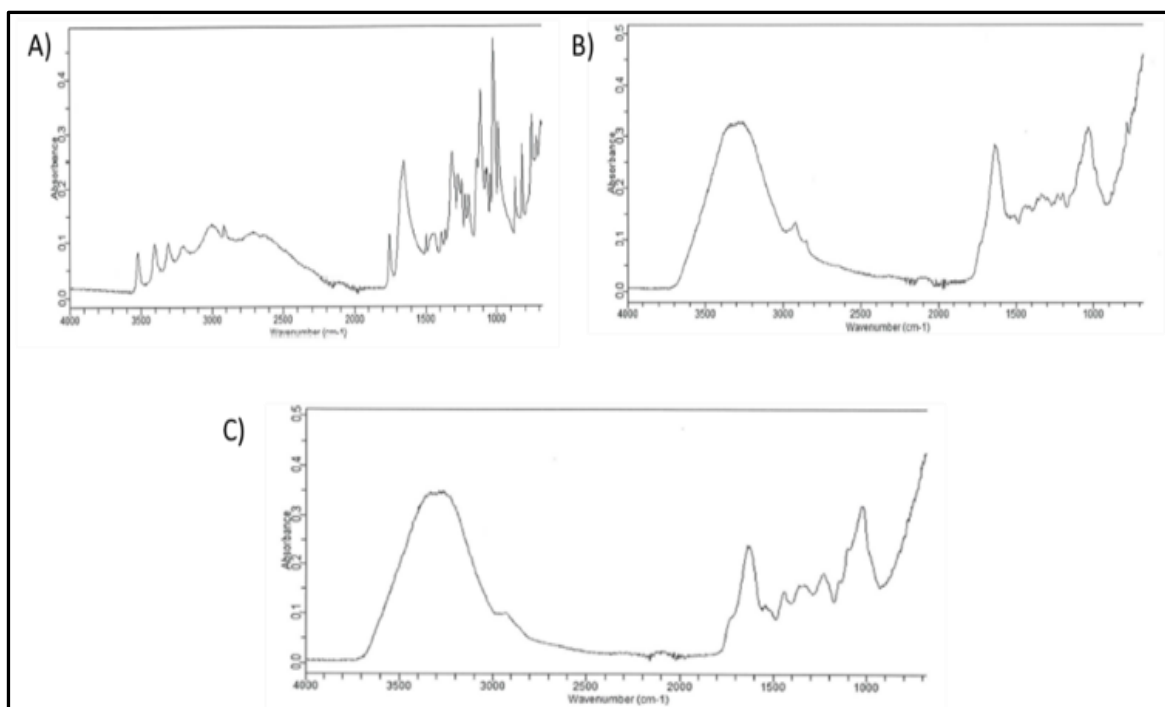


Fig. 1 A) Chromatogram of standard Ascorbic acid B) Chromatogram of *R. sanctus* C) Chromatogram of *C. mas*

3.2 Yeast Ethanol Fermentation

The fermented samples were checked for ethyl alcohol presence. The presence of ethyl alcohol was detected as a result of the analysis. The standard retention time of ethyl alcohol is 4.289. Ethyl alcohol was found in both concentrations of fermented *C. mas* and *R. sanctus* samples (Table 2).

Table 2 Ethyl Alcohol Determination in the Fermented Fruit Samples

Fermented Samples	Retention Time	Area
<i>Rubus Sanctus</i> - N1	4.371	14064
<i>Rubus Sanctus</i> - N2	4.329	11148
<i>Cornus Mas</i> -N1	4.395	24074
<i>Cornus Mas</i> -N2	4.364	22078

3.3 Antimicrobial Activity Analysis

In the analysis of the antifungal activity determination of the fermented samples, the growth was observed immediately on the first day, observed up to day 5. Reproduction has increased day by day.

The fermented *C. mas* and *R. sanctus* samples were evaluated for antibacterial activity against strains of *P. aeruginosa* and *S. aureus* microorganisms. Transparent inhibition zones where no growth is seen were identified in the petri dishes at the end of 24 hours (Table 3). The antibacterial activity determination results of the fermented *C. mas* and *R. sanctus* samples are given in image 1.

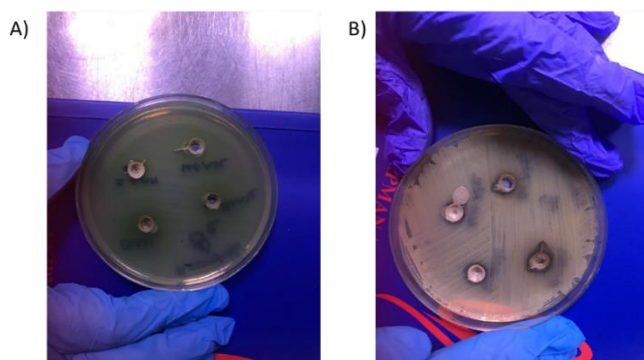


Image 1 Results of the antibacterial effect of A) *P. aeruginosa* B) *S. aureus*

Table 3 Inhibition zone diameters of fermented and non-fermented samples against selected bacteria (mm)

Samples	Unfermented	Fermented (average)
<i>Rubus Sanctus</i> -N1	-	10.8 mm(<i>P. aeruginosa</i>)
<i>Rubus Sanctus</i> -N2	-	11.1 mm (<i>S. aureus</i>)
<i>Cornus Mas</i> -N1	-	11.3 mm (<i>P. aeruginosa</i>)
<i>Cornus Mas</i> -N2	-	10.5 mm(<i>S. aureus</i>)

3.4 Antioxidant Activity Analysis using DPPH, CUPRAC and Folin Ciocalteu Methods

The antioxidant activity determination analysis results of the samples are given in Fig 2, 3 and 4.

4 Discussion

Berry fruits are attracting attention for their beneficial effects on the human gut flora due to their high antioxidant contents. They have preventive advantages on diseases including cancer, cardiovascular, and intestinal (Olas 2018). In our study, the antioxidant, antifungal and antimicrobial effects of the fermented extracts of *C. mas* and *R. sanctus* berry fruits were analysed. The fruits were collected in province of Bartın in the Western Black Sea region of Türkiye. Initially, the fruit samples were examined to determine if there were any pesticide residues present. Since pesticides can have harmful consequences on health, the identification of pesticide residues, especially in foods, has been the focus of many studies (Damalas and Eleftherohorinos 2011). The fruit samples were prepared following protocols and the presence of pesticide residue was checked for 58 parameters in the GC-MS device. There was no evidence of pesticide residue. In addition, the presence of ascorbic acid (Vitamin C), which is an antioxidant and a necessary nutrition for humans (Beyer 1994), was detected in the IR-FTIR analysis before the fermentation of the samples. Previous studies also suggest high ascorbic acid contents for the *Rubus* genus (Ponder and Hallman 2020). Subsequently, aqueous extracts prepared from *C. mas* and *R. sanctus* fruits were fermented with *S. cerevisiae*. The presence of ethyl alcohol was verified using the GC-FID device. The amount of ethyl alcohol was higher in the fermented samples of *C. mas*. *S. cerevisiae* was able to reproduce in these fruit extracts and could ferment the samples. Song and coworkers have applied *S. cerevisiae* to improve *Rubus coreanus* Miquel vinegar fermentation process (Song et al. 2019). This application has accelerated the fermentation process.

Antioxidant activity of the fermented samples was analysed using CUPRAC, DPPH and Folin Ciocalteu methods. *R. sanctus* fermented samples at both concentrations showed higher antioxidant capacity values than *C. mas* in the CUPRAC and Folin Ciocalteu analysis results. In the DPPH antioxidant activity determination analysis, the fermented *C. mas* samples with a concentration of 1mg/ml gave higher results than *R. sanctus*, the situation was the opposite in the samples prepared with a concentration of 0.5 mg/ml. The reason for the deviation may be analytical, sample preparation and instrument related. Prior research has also revealed that *Rubus Sanctus* and *Cornus Mas* has greater antioxidant levels (Tiptiri-Kourpeti et al. 2019; Zengin et al. 2020). A very recent research has demonstrated the antioxidant and antimicrobial activity of *C. mas* fruits (Aurori et al. 2023). Additionally, a recent study examined the antioxidant and antibacterial properties of both unfermented *C. mas* fruits and fermented *C. mas* fruits using kombucha (Zagórska-Dziok, 2023). In comparison to the extract, they found that the ferment had greater activity, which supports the validity of employing a fermentation agent may produce valuable products. Though to the best of our knowledge there is no study that involves both fruits.

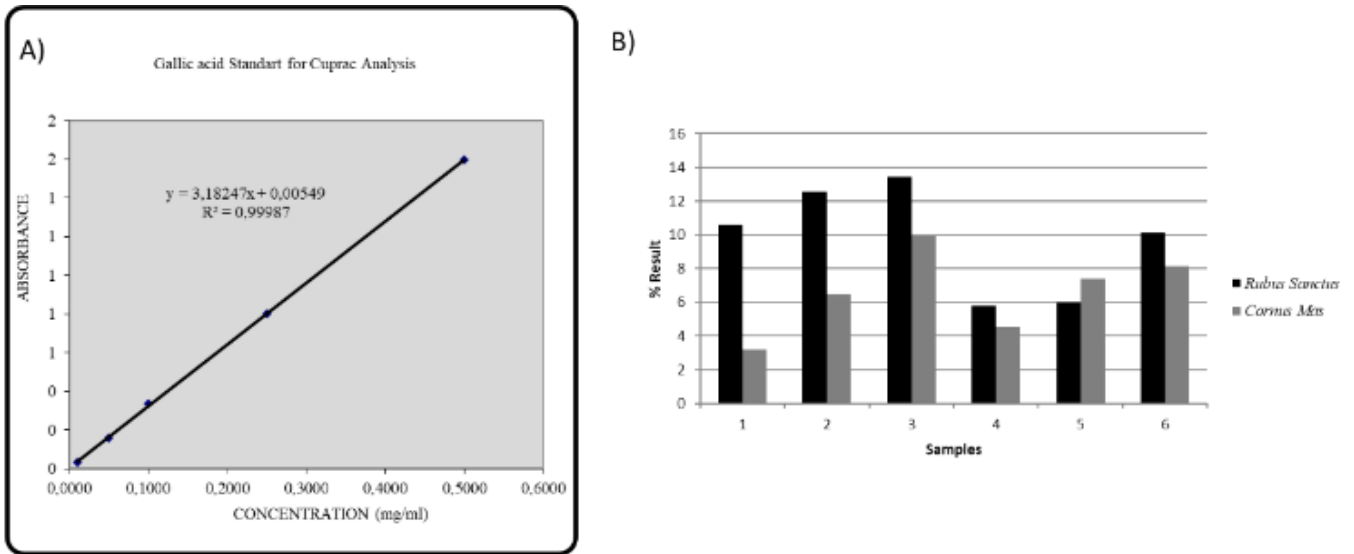


Fig. 2 A) Linearity study of gallic acid standard B) Graphical comparison of antioxidant capacity results of *C. mas* and *R. sanctus* using CUPRAC method.

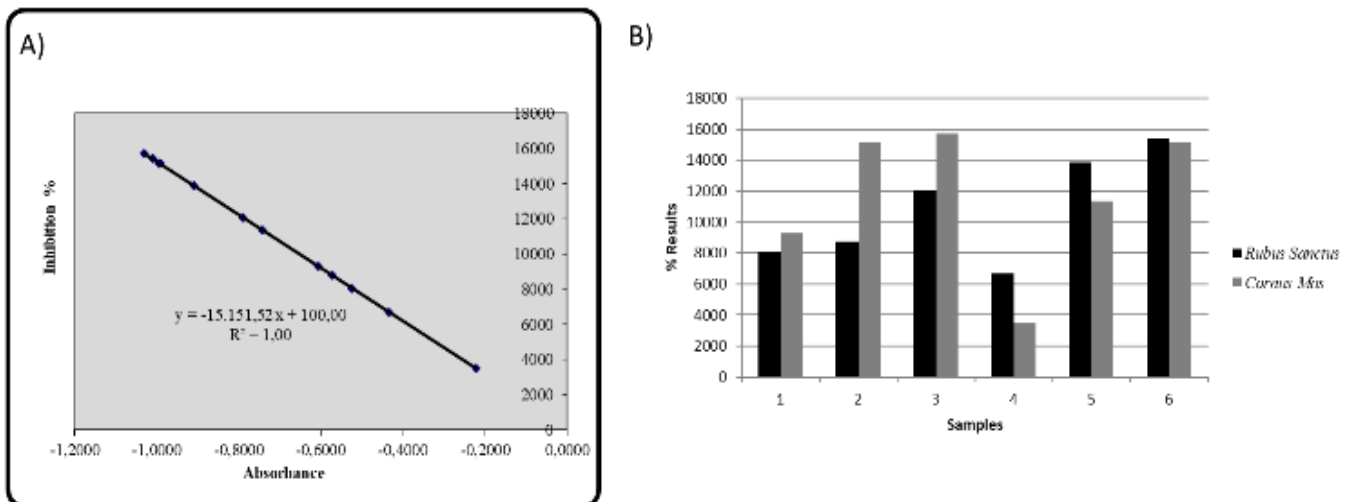


Fig. 3 A) The inhibition effect of the concentration of antioxidant compounds in the samples on the DPPH solution, B) Graphical comparison of antioxidant capacity results of *C. mas* and *R. sanctus* using DPPH method.

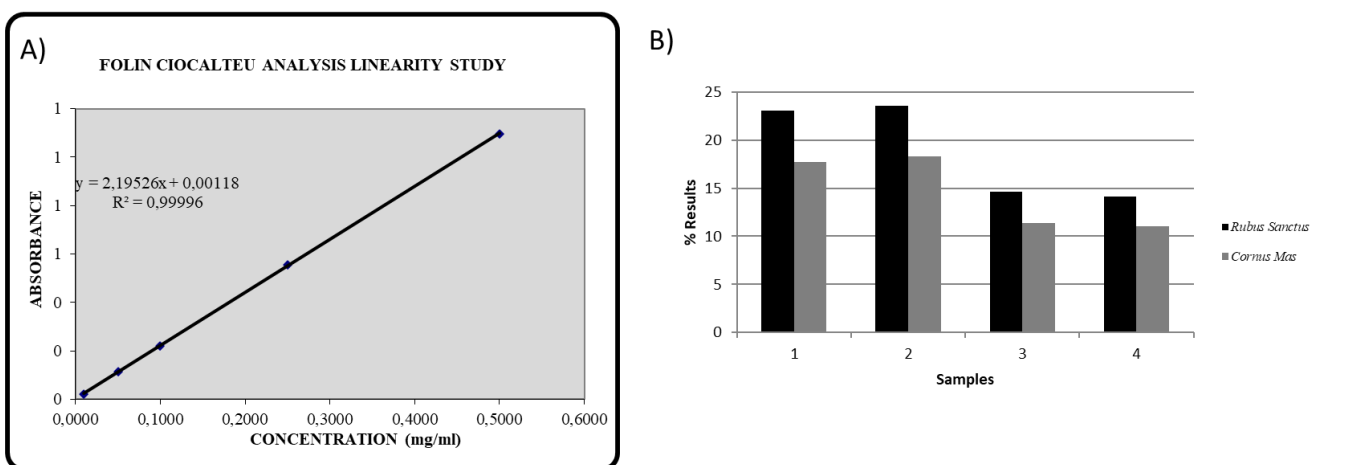


Fig. 4 A) Linearity study of gallic acid standard, B) Graphical comparison of antioxidant capacity results of *C. mas* and *R. sanctus* using Folin Cioaltea method

Phenolic compounds found in fruits and vegetables show antibacterial effect by inhibiting the proliferation of microorganisms. *P. aeruginosa* and *S. aureus* were used to check for antibacterial activity, and *C. albicans* was used to check for antifungal activity of the fermented samples. The transparent inhibition zones where no growth is seen is greater in *C. mas* samples. Though Zagórska-Dziok (2023) study has identified high antimicrobial activity with kombucha fermented *C. mas* fruits, in our study the fermented samples do not suppress *P. aeruginosa* and *S. aureus* greatly. This may be a result of a lower than needed concentration of the fermented samples. The fermented samples were not effective on *C. albicans* as well, and reproduction begins and continues after 24 hours from the first day.

5 Conclusion

Fresh fruit is preserved longer by fermentation, which may allow us to reap their benefits over a longer period. In this study, *R. sanctus* and *C. mas* fruits harvested from the Western Black Sea Region of Türkiye were fermented and their antioxidant and antibacterial activities were analyzed. Fermented *R. sanctus* samples at both concentrations showed higher antioxidant capacity values than *C. mas* in the CUPRAC and Folin Ciocalteu analysis results. Further experiments may be done using different combinations of *R. sanctus* and *C. mas* together or with different fruits, fermenting longer, changing the fermentation steps.

Acknowledgements

This research did not receive any specific grant from funding agencies in the public, commercial, or not-for-profit sectors

Authors' contributions:

DÜ: data collection, analysis and interpretation of results, and manuscript preparation TS: study conception and design, manuscript preparation, manuscript review

Conflict of interest disclosure:


The authors have no conflict of interest

References

- Apak R, Güçlü K, Demirata B, Özyürek M, Çelik SE, Bektaşoğlu B, Berker KI, Özyurt D. (2007) Comparative evaluation of various total antioxidant capacity assays applied to phenolic compounds with the CUPRAC assay. *Molecules* 12(7). doi:10.3390/12071496
- Aurori M, Niculae M, Hanganu D, Pall E, Cenariu M, Vodnar DC, Bunea A, Fiț N, Andrei S (2023) Phytochemical Profile, Antioxidant, Antimicrobial and Cytoprotective Effects of Cornelian Cherry (*Cornus mas* L.) Fruit Extracts. *Pharmaceuticals* (Basel) 16(3):420
- Bayer A, Kirby W, Sherris J, Turck M (1966) Antibiotic susceptibility testing by a standardized single disc method. *Am J Clin Pathol* 45(4):493-496.
- Beyer RE (1994) The role of ascorbate in antioxidant protection of biomembranes: interaction with vitamin E and coenzyme Q. *J Bioenerg Biomembr.* 26(4):349-58
- Collins C (2004) Collins and Lyne's Microbiological Methods. 8 ed. USA: CRC Press, 175-190
- Damalas CA, Eleftherohorinos IG (2011) Pesticide exposure, safety issues, and risk assessment indicators. *Int J Environ Res Public Health.* 8(5):1402-1419
- Gulcin İ (2020) Antioxidants and antioxidant methods: an updated overview. *Arch Toxicol* 94(3). doi:10.1007/s00204-020-02689-3
- Lobo V, Patil A, Phatak A, Chandra N (2010) Free radicals, antioxidants and functional foods: Impact on human health. *Pharmacogn Rev* 4(8) doi:10.4103/0973-7847.70902
- Lussignoli S, Fraccarolli M, Andriolli G, Brocco G, Bellavite P (1999) A microplatebased colorimetric assay of the total peroxy radical trapping capability of human plasma. *Analytic Biochemistry* 269:38-44.
- Olas B. (2018) Berry Phenolic Antioxidants - Implications for Human Health? *Front Pharmacol* 9:78
- Ponder A, Hallmann E (2020) The nutritional value and vitamin C content of different raspberry cultivars from organic and conventional production, *Journal of Food Composition and Analysis*, 87,103429
- Sanchez-Moreno C, Larrauri JA, Saura-Calixto F (1999) Free radical scavenging capacity of selected red, rose and white wines. *J Sci Food Agri* 79:1301-1304.
- Song NE, Jeong DY, Baik SH (2018) Application of indigenous *Saccharomyces cerevisiae* to improve the black raspberry (*Rubus coreanus* Miquel) vinegar fermentation process and its microbiological and physicochemical analysis. *Food Sci Biotechnol* 28(2):481-489.
- Soong YY, Barlow PJ, Tamez Uddin M, et al. (2019) Bioactive Molecules in Food. Vol 65.
- Şanlıer N, Gökçen BB, Sezgin AC (2019) Health benefits of fermented foods. *Crit Rev Food Sci Nutr* 59(3). doi:10.1080/10408398.2017.1383355
- Tiptiri-Kourpeti A, Fitsiou E, Spyridopoulou K, Vasileiadis S, Iliopoulos C, Galanis A, Vekiari S, Pappa A, Chlichlia K (2019) Evaluation of Antioxidant and Antiproliferative Properties of *Cornus mas* L. Fruit Juice. *Antioxidants* (Basel). 8(9):377
- Zagórska-Dziok M, Ziemlewska A, Mokrzyńska A, Nizioł-Łukaszewska Z, Sowa I, Szczepanek D, Wójciak M (2023) Comparative Study of Cytotoxicity and Antioxidant, Anti-Aging and Antibacterial Properties of Unfermented and Fermented Extract of *Cornus mas* L. *Int J Mol Sci* 24(17):13232
- Zengin G, Ferrante C, Senkardes I, Gevrenova R, Zheleva-Dimitrova D, Menghini L, Orlando G, Recinella L, Chiavaroli A, Leone S, Brunetti L, Nancy Picot-Allain CM, Rengasamy KRR, Mahomoodally MF (2019) Multidirectional biological investigation and phytochemical profile of *Rubus sanctus* and *Rubus ibericus*. *Food Chem Toxicol* 127:237-250

Bulletin of Biotechnology

ERRATUM: Microwave-assisted green biosynthesis of gold nanoparticles from *Eriobotrya japonica* leaf extract

Gönül Serdar* 

*Karadeniz Technical Universty, Central Research Laboratory, Trabzon, Turkey.

*Corresponding author : gonulserdar@ktu.edu.tr
Orcid No: <https://orcid.org/0000-0002-3589-2323>

Received : 08/12/2021
Accepted : 23/12/2021

Abstract: Due to inaccuracies in the abstract section of the article titled “Microwave-assisted green biosynthesis of gold nanoparticles from *Eriobotrya japonica* leaf extract”, published in the second issue of the Bulletin of Biotechnology in 2021 on pages 38-43, a re-editing process has been undertaken. The relevant abstract editing has been carried out. This correction text is provided with the aim of rectifying the mistake present in the article.

The original version of this article was published on December 31, 2021. Link: <https://dergipark.org.tr/en/pub/biotech/issue/67327/1034330>.

Keywords: Gold nanoparticle, *Eriobotrya japonica* Leaf, MAE.

Bulletin of Biotechnology

Challenges in optimizing 3D scaffold for dentin-pulp complex regeneration

Rola Zahedah^{1*} , Bircan Dinç² 

¹*Department of Tissue Engineering and Regenerative Medicine, Bahcesehir University, Istanbul, Turkey*

²*Department of Biophysics, School of Medicine, Bahcesehir University, Istanbul, Turkey*

*Corresponding author: rola.amro@gmail.com
Orcid No: <https://orcid.org/0000-0003-3681-157X>

Received : 25/01/2023
Accepted : 10/12/2023

Abstract: Regenerating dentin-pulp complex (DPC) using tissue engineering offers a novel and promising therapeutic alternative for restoring teeth. A crucial component of such a therapy is the designing and fabrication of an appropriate 3D Scaffold. In this review, we set out to highlight some of the general challenges associated with optimizing the most suitable scaffold for DPC regeneration to develop "biomimetic" approaches that influence stem cell proliferation, differentiation, and angiogenesis. It is essential to comprehend the biology and physical features of the dentin-pulp complex with updated bionanotechnology to overcome the limitations of biomaterials to address the challenges in manufacturing the optimal scaffold. To date, current scaffolding models fail to regenerate a whole tooth. The success of regenerative dentistry relies on stem cells and scaffolds may shape the future of dental treatment.

Keywords: Tissue engineering ;3D scaffold; Pulp dentin complex; Regenerative dentistry; Stem cell therapy

© All rights reserved.

1 Introduction

Tissue engineering is an interdisciplinary topic that combines cell biology understanding, biotechnology, biomaterials, and appropriate biochemical components to manufacture replica organs and tissues or to restore damaged tissues (Langer 2007; O'Brien 2011). It necessitates seeding cells onto such a scaffold, which is then grown in vitro before being transplanted into the body when matured (Rabkin and Schoen 2002) following that, normal tissue regeneration processes occur, blood vessels enter the structure, and angiogenesis is completed (Noohi et al. 2022) and the scaffold finally dissolves, degradation results in newly regenerated tissue in the site (Li et al. 2019). That's why it is important to first understand and replicate tissues' dynamic processes to repair injured tissues and organs (Jain and Bansal 2015; Gritsch et al. 2019). It wasn't until the late 1980s that the term "tissue engineering" entered the terminology. Synthetic biodegradable materials are often known as scaffolds. The scaffold replicates the in vivo environment by providing a three-dimensional area for cell growth (Almutairi et al. 2019). These synthetic matrices may be built to any shape and include growth agents to differentiate cells into the right tissue types as shown in the steps of Figure 1 (Huang 2009).

Over the past two decades, tissue engineering has advanced in biodegradable scaffolds, integration of cells and biopolymers to create tissue engineering constructs, bioreactors that stimulate cultured tissues with developmentally relevant signals, and characterization and isolation of adult and embryonic stem cells (Qu et al. 2015; Diana et al. 2020). Clinical advancements have occurred with skin and cartilage, which are simple to replace. Despite these successes, many obstacles remain (Liu et al. 2007).

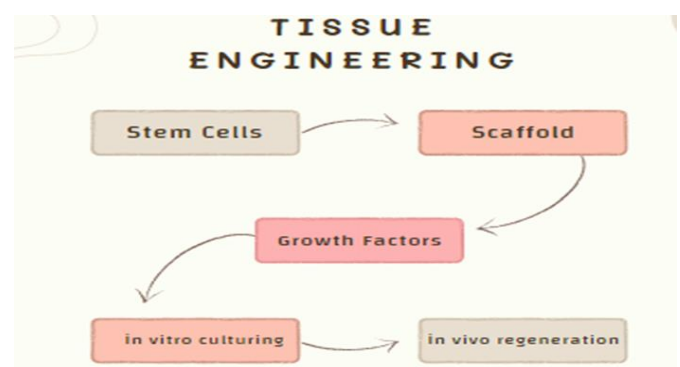


Fig 1. Tissue engineering procedure.

2 Tissue Engineering Scaffold features

The scaffold supports cell attachment, proliferation, differentiation, and extracellular matrix (ECM) formation. ECM plays a role in cell-to-cell interactions and tissue architecture. Scaffolds shuttle cells, growth factors, as well as biomolecular signals (Agrawal and Ray 2001; Chan and Leong 2008; Zhang et al., 2019).

Scaffolds, a crucial part of the tissue engineering concept, address tissue creation by providing cells with a suitable environment in which to adhere, proliferate, differentiate, and produce their extracellular matrix (O'Brien 2011).

Generally, the optimum scaffold should have distinctive features. First, cell migration and division are facilitated by a dense network of linked holes attached throughout the scaffold's interior. Porous structures with channels allow for the efficient transport of oxygen and the amount of nutrients to cells at different depths within the scaffold, as well as the removal of metabolic waste. Biocompatibility requires just a tight fit for cells to attach and grow, designed to the required tissue. An adequate biodegradation rate and the right amount of mechanical strength and physical characteristics are other substantial properties. Utilizing such a scaffold would greatly benefit tissue engineering and regeneration. Biomaterials utilized in tissue engineering scaffold manufacturing may be broadly classified as synthetic or natural sources, or semisynthetic materials (Griffith and Naughton 2002; Liu et al. 2007; O'Brien, 2011; Eline et al. 2022).

To yet, tissue engineering products have only been successful in thin structures (skin) and tissues without a blood supply (cartilage) (Cao et al. 2006). However, several strategies are being studied for the development of scaffolds to compensate for deficiencies in other tissues.

The primary prerequisites for biomaterials used as scaffolds include biocompatibility as well as adequate surface characteristics to promote cell adhesion, proliferation, and differentiation (Dhandayuthapani et al. 2011; Leite et al. 2021).

For scaffold production in diverse tissue engineering applications, synthetic biomaterials (bio-ceramics & biopolymers) are the most commonly used (Liu et al. 2007). Natural or manufactured synthetic biomaterials also serve as scaffolding. Porosity, mechanical properties stability feasible application for clinical treatment are all important features of an optimal scaffold for successful tissue regeneration (Palma et al. 2017).

In literature, pulp tissue regeneration failed in the 1960s and 1970s. Tissue-engineering approaches in the late 1990s re-evaluated pulp tissue regeneration (Huang 2009). In immunocompromised mice, Gronthos et al. showed that pulp cells may form dentin (Gronthos et al. 2000) this discovery illuminated therapeutic pulp dentin regeneration.

In the last decade, the pulp-dentin complex and its regeneration have grown in relevance and complexity. To date, several biomaterial scaffolds from various cell sources have been suggested to regenerate natural extracellular matrix

(ECM) analogs. Adequate mechanical qualities and the capacity to promote cell adhesion and proliferation are prerequisites for a successful dental scaffold design (Zhang et al. 2013; Grawish et al. 2020; Iranmanesh et al. 2022).

The present study aims to draw attention to some of the challenges that arise when we want to figure out the optimal scaffold to regenerate the dentin pulp complex.

3 Scaffolds to regenerate dentin-pulp complex

Prosthetics and implants with prosthetic crowns are the main dental treatments for missing teeth. The prostheses don't remodel like normal teeth. Nowadays the demand uses of postnatal dental stem cells on a bioengineered three-dimensional framework to regenerate tooth organogenesis is increasing (Zhang et al. 2013).

In teeth, pulp and dentin are considered histologically as two different tissues functionally as one entity (Linde and Goldberg 1993).

Dentin, nerves, as well as blood vessels, are all produced by odontoblast cells throughout development. While dentin and pulp feature separate in their structures and compositions once formed, they remain responsive to signals as just a single entity. Dentin exposure caused by attrition, trauma, or caries causes severe pulpal responses that lower dentin permeability and encourage dentin production, the alteration of fibroblasts, nerves, blood vessels, odontoblasts, leukocytes, and immune systems triggers these responses (Goldberg and Smith 2004; Tsou et al. 2017).

Recent findings of the impact of nerves upon the pulp's blood vessels conversely have given us a more complete understanding of how they interact depending on the dentin's response to the stimulus. Too frequently in works of literature, the various components of the pulp-dentin complex are investigated separately. However, the separate components are highly interacting, with each moderating the performance of the others. While delving into the intricacies of the pulp-dentin complex may pose challenges in the realm of research, it nonetheless presents an exceptional and distinctive backdrop for scholarly inquiry.

Scientists use multidisciplinary methodologies to address the challenges related to the pulp-dentin complex. Twenty years ago, the finding of stem cells in dental pulp opened the possibility for the regeneration of dentin pulp complex (Gronthos et al. 2000).

Some consider the predicted regeneration of the dentine-pulp complex to be the "golden standard" of regenerative research, however, this has yet to be accomplished. One of the challenging targets in regenerating the complex is gaining the unique tubular design that is only found in the calcified natural dentin (Tsou et al. 2017).

Most of the dentin pulp complex regeneration literature lacks definitive data on the optimal biomaterial scaffold, leaving the field open to trial-and-error approaches. The proper biomaterials are essential for regenerating teeth to function like the original. The literature evaluation also lacks pulp tissue material characteristics data (Ozcan et al. 2016).

4 Difficulties Associated with Utilization Scaffolds in Dental Regeneration

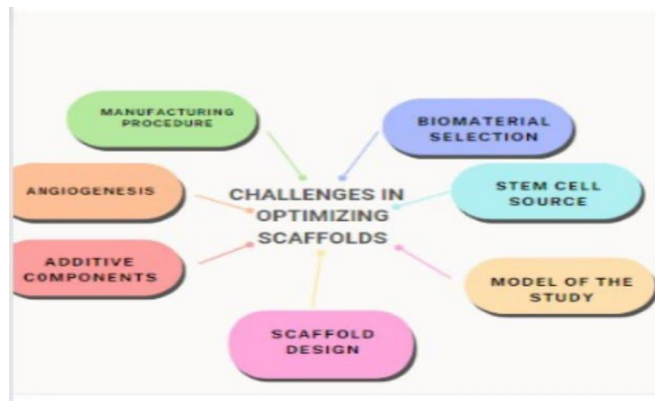


Fig 2. The main challenges in utilizing an optimal scaffold.

The most challenging aspect of finding the optimal scaffold is selecting the suitable biomaterial that will be employed. Recent works of literature contain material suggestions and primary assessments (Farag 2022).

Blood clots have been used as scaffolds for some studies (Vail et al. 1999). However, numerous scaffolds—natural polymers (collagen, fibrin, chitosan, alginate) or synthetic polymers (PGA, PLGA, PLA). Synthetic biopolymers are more versatile and predictable than natural materials. Several studies also focused on FDA-approved synthetic biopolymers. Polylactic acid (PLA) and poly-glycolic acid (PGA) are the most often studied biodegradable polymers (Leite et al. 2021; Eline et al. 2022).

Degradation and by-products are one of the limitations of synthetic polymers (PLA, PGA, PLGA, PLLA) that disintegrate rapidly after implantation. Polymers lose molecular weight in liquids. Mass loss can't occur until molecular chains are small enough to diffuse out of the polymer matrix. Acidic by-products release gradient-wise with mass loss. The observed transitory abnormalities may be caused by a massive release of acidified breakdown and resorption by-products, which may cause inflammatory reactions in vivo if the adjacent tissue has inadequate vascularization or metabolic activity (Hutmacher 2000; Anderson 2001; Rodrigues et al. 2016). Tissue-engineered products may be impeded by inflammation and foreign body reactions.

Incorporating ceramics like hydroxyapatite (HA) particles into a polymer matrix creates a composite scaffold with decreased local inflammatory reactions was one of the overcoming. HA's basic resorption affects buffer polymers' acidic degradation by-products, shielding cells from a hazardous environment (Kempen et al. 2006). Coating by such particles should not impair the polymer's mechanical qualities or biocompatibility.

The model, cell exclusion approaches, stem cell potentials, micro-environment, teeth, in situ microcirculation, surgical process, and biomaterials are all factors that affect study outcomes. inflammation may also hinder neo-angiogenesis and mineralized tissue development, which contribute to regeneration defects (Peters et al. 2021).

Acellular alternatives have been created to avoid cell transplantation's drawbacks. Acellular approaches emphasize cell recruitment with full pulp regeneration relying on periapical cells. Trope achieved the most clinical improvement utilizing this strategy. After cleaning the canal, instrumenting into the peri-apical region creates a blood clot. The blood clot forms new tissue and stores natural biomolecules that attract new cells (Trope 2010).

In creating an artificial organ, biomaterial surfaces have become essential (Leite et al. 2021). Biodegradable scaffolds bring cells together for microenvironments, scaffolds are optimized for physical, mechanical, biochemical, and biological qualities. Voltage may be used to create surfaces with dynamic interfacial properties, including wettability. Surface-confined, single-layered molecules translate between hydrophilic and moderately hydrophobic states to modify wetting behavior (Langer 2007; Hollister and Lin 2007).

A decellularized matrix with specified trophic element distribution is intriguing. Extracellular matrix-based scaffolds have modulated the host response, attracted progenitor cells, and stimulated constructive remodeling in recent investigations. A decellularized matrix attracts stem cells and progenitors. Regeneration in those investigations parallels natural cell recruitment from neighboring tissues to the new ECM network (Peters et al. 2021).

The ubiquitous need for creating blood perfusion via engineered tissues of clinically meaningful met by tissue vascularization which can be utilized to initiate or restore blood flow is another challenge (Langer 2007) sustained release of angiogenic factors through scaffolds, seeded endothelial cells straight into the scaffold, and designing vasculature directly into tissue via microfabrication are promising approaches to this challenge (Noohi et al. 2022).

Stem cell sources are a significant challenge in the field of dental tissue engineering. Dental pulp stem cells found in permanent and deciduous teeth may be exploited for tissue engineering. The first effective attempt to build complex tooth designs using single-cell solutions separated from swine third molar tooth bud showed dental pulp stem cells throughout this tissue (Gronthos et al. 2000) Since then, similar methods using self-dental pulp stem cells as bioengineered organs for regenerative investigations are an option.

Sharpe and Young (2015) demonstrated that both non-dental and dental adult stem cells have the capability to generate mouse teeth, emphasizing the potential utility of non-dental stem cells in dental research.

Mesenchymal stem cells from the root apical papilla were shown to rebuild tooth strength and appearance (Cordeiro et al. 2008). However, cell differentiation and stem cell sources require further research.

Tissue engineering of the dentin-pulp complex presents several challenges when using 3D scaffolds. Scaffolds must do more than support cells mechanically to resemble the extracellular matrix. It must also be bioactive and dynamic, regulating cellular activity and intercellular communication (Gong et al. 2016). Electrospinning, gas foaming, melt

molding, freeze-drying, solvent casting, particle leaching, and phase separation are traditional scaffolding processes that cannot be accurately controlled (Peters et al. 2021).

Processes such as choosing the biomaterial with appropriate physicochemical properties, producing the designed scaffold, and then monitoring the response in the tissue have separate difficulties and risks (Figure 2).

5 3D printed scaffold challenges dental regeneration

Another crucial challenge in optimizing the scaffold is the manufacturing procedure. Recent years have seen the introduction of additive manufacturing methods like 3D printing into the field of tissue engineering (Noohi et al. 2022). The idea of 3D bioprinting stems from Charles Hull's development of stereolithography in 1986. Customized cell-laden scaffolds are the result of 3D bioprinting. Cells may be placed with pinpoint accuracy using 3D bioprinting (Figure 3). It may be employed for high throughput manufacture and provides fine control over scaffolds' exterior and interior morphology. Because of its porous interior, the 3D-printed scaffold can allow nutrients and oxygen to reach the cells inside it, promoting healthy cellular metabolism (Peters et al. 2021).



Fig 3. The 3D dental bioprinting procedure

Endodontic regeneration bioprinting options include inkjet bioprinting, laser-assisted bioprinting (LAB), as well as extrusion bioprinting (Figure 4) which are the main types of 3D bioprinting (Iranmanesh et al. 2022). Relatively common 2D desktop inkjet printers have helped popularize the printing process known as "inkjet printing." Droplets of biomaterials are ejected from the nozzle of an inkjet printer through either heat energy or a piezoelectric actuator. It's easy to use, produces high-quality results, and won't break the bank: thermal inkjet technology. Yet, bio-tendency inks to clog nozzles is a significant drawback of this technique. As a result of gelation, droplets are not uniform in size, which might pose problems during the printing process. Another difficulty arises from the fact that the heat and shear stress caused by making bio-ink drops might affect cell viability (Matai et al. 2020).

In LAB, laser pulses at a donor slide propel cell-loaded hydrogel droplets toward a collection slide (Vijayavenkataraman et al. 2017). LAB makes heterogeneous tissue structures with high precision (10-100 m), a broad variety of sizes, and high cell density. Automation, reproducibility, and high productivity make LAB a potential 3D tissue creation process. Biomaterials must cross-link

quickly, so should be chosen carefully. Laser wavelength must preserve cell and biomaterial resolution in 3D printed constructs (Matai et al. 2020). However, manufacturing time and high-pressure homogenization of cells in solution are major concerns (Peters et al. 2021).

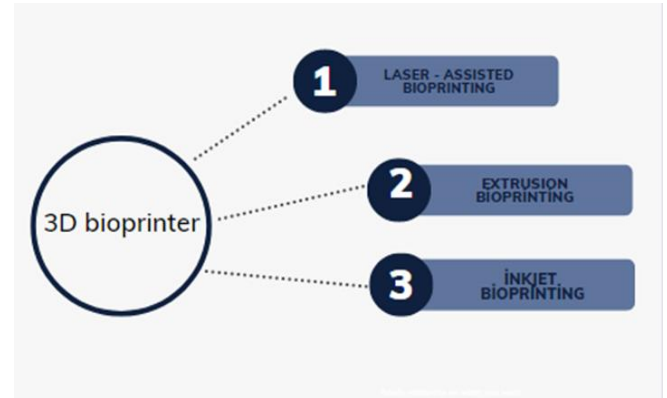


Fig 4. The main type of 3D bioprinter

Extrusion bioprinters propel biopolymers or cell-laden hydrogels via a nozzle using air pressure or mechanical devices like pistons or screws. Extrusion bioprinters with several printer heads may deposit multiple bio-inks without cross-contamination. They enhance printed structure porosity, shape, and cell dispersion. Extrusion bioprinting for tissue engineering scaffolds is becoming more popular due to its versatility (Matai et al. 2020; Peters et al. 2021; Iranmanesh et al. 2022)

Despite its rising popularity due to its benefits and uses in other medical sectors, only a few research publications have been published on 3D bioprinting for endodontic regeneration. 3D bioprinting for dental regeneration is yet to be optimized. Use which bioprinter technology? Which bio-ink is better for endodontics? Which method—fabricating dental pulp, tissue structures, enamel, cement, and ligament—would provide the greatest results? These printers employ cell-laden hydrogels, extracellular matrix, or cell aggregation bio-inks. These materials don't imitate dentine and pulp's intricate extracellular matrix. Bio-inks that regenerate tissues, especially odontogenic ones, may help regenerative dentistry grow.

Bio-ink odontogenic and cytocompatibility have been studied lately. The differentiation and proliferation of DPSCs in a regular Alg-Gel hydrogel (Alginate-gelatine) was compared to the scaffold to a 3D bioprinted scaffold extract. 3D-printed Alg-Gel scaffolds develop and adhere faster than conventional ones. Seeded DPSCs show increased proliferation and osteogenic/odontoblastic differentiation potential because 3D-printed Alg-Gel scaffold extracts contain more phosphorus and calcium (Yu et al. 2019).

Cell-loaded collagen-based bio-inks with the necessary biological properties and structure may be bioprinted in the root canal. A portable drop-on-demand bioprinter was utilized to test ex vivo human teeth. Vasculogenesis, the production of new blood vessels, was shown to be qualitatively and quantitatively identical to collagen, fibrin, and non-bio-printable hydrogel controls (Duarte Campos et al. 2020).

In studies for complete tooth regeneration, tooth-like tissues and structures with different properties have been created. Research data showed that smaller sizes of dental tissue could be produced instead of the entire crown of the tooth. Dental germ culture is difficult (Li et al. 2019) and scaffold-based methods are unsuited for tooth-like tissue regeneration because they can't pre-define the positioning of many cell types (Peters et al. 2021).

Dentine-pulp complex reconstruction using 3D bioprinting is new. Before they can be used securely and cost-effectively, the approaches require additional study and development. Most evidence comes from in vivo and ex vivo models, which do not account for diagnostic and therapeutic parameters, microorganisms and their by-products, dentin's inherent structure, or the impact of irrigant solutions on the remaining dentin. No controlled clinical studies of these regenerative dental treatments have been done (Peters et al. 2021; Iranmanesh et al. 2022).

6 Conclusion

It is essential to comprehend the biology and physical features of the dentin-pulp complex with updated bionanotechnology to overcome the limitations of biomaterials in order to address the challenges in manufacturing the optimal scaffold. Utilizing components that contribute to normal tooth function and structure must comprehensively address the difficulties of generating a dentin-pulp complex that resembles the natural tissues to reach the whole bioengineered tooth.

Since stem cells are employed in dentin pulp complex regeneration research, procedures should be given more attention. Bacteria may influence regeneration procedure outcomes.

Some stem cells are more susceptible to apoptosis and immune-mediated cell death. Thus, it is unclear whether these cell types may be exploited similarly. Stem cell characteristics and interactions require further study. Stem cells interact differently with the immune system. This knowledge is crucial for regenerative medicine. Stem cell treatment may be harmful if stem cells generate proinflammatory cytokines. The current scaffolding models for pulp dentin complex regeneration fail to account for the important variations between pulp and dentin and are thus unable to regenerate a whole tooth. However, in studies for regenerative endodontic treatment, the most effective results are obtained with stem cell research. There is a need for further research in the field to get complete regeneration, and address the challenges, overcoming the limitations in previous studies. Finding the optimal scaffold may alter the future of dental treatment methods. The bioengineered future is bright, and what we discover about stem cells and scaffolds today will shape it.

References

- Agrawal CM, Ray RB (2001) Biodegradable polymeric scaffolds for musculoskeletal tissue engineering. *J Biomed Mat Res* 55(2):141-150
- Almutairi W, Ghaeth H, Yassen, Anita Aminoshariae, Kristin A. Williams, Andre Mickel (2019) Regenerative endodontics: a systematic analysis of the failed cases. *J Endod* 45(5):567-577
- Anderson JM (2001) Biological responses to materials. *Annual review of materials research* 31(1):81-110
- Bergenholtz G, Mjör I, Cotton W, Hanks C, Kim S, Torneck C, Trowbridge H (1985) Consensus report. *J Dent Res* 64(4):631-633
- Cao Y, Mitchell G, Messina A, Price L, Thompson E, Penington A, Morrison W, O'Connor A, Stevens G, Cooper-White J (2006) The influence of architecture on degradation and tissue ingrowth into three-dimensional poly (lactic-co-glycolic acid) scaffolds in vitro and in vivo. *Biomater* 27(14):2854-2864
- Chan BP, Leong KW (2008) Scaffolding in tissue engineering: general approaches and tissue-specific considerations. *Eur Spine J* 17(4):467-479
- Cordeiro MM, Dong Z, Kaneko T, Zhang Z, Miyazawa M, Shi S, Smith AJ, Nör JE (2008) Dental pulp tissue engineering with stem cells from exfoliated deciduous teeth. *J Endod* 34(8):962-969
- Diana R, Ardhani R, Kristanti Y, Santosa P (2020) Dental pulp stem cells respond on the nano topography of scaffold to regenerate dentin-pulp complex tissue. *Regen Therapy* 15:243-250
- Dhandayuthapani B, Yoshida Y, Maekawa T, Kumar DS (2011) Polymeric scaffolds in tissue engineering application: A review. *Int J Polym Sci* 2011
- Duarte Campos DF, Zhang S, Kreimendahl F, Köpf M, Fischer H, Vogt M, Blaeser A, Apel C, Esteves-Oliveira M (2020) Hand-held bioprinting for de novo vascular formation applicable to dental pulp regeneration. *Connect Tissue Res* 61(2):205-215
- Elline, Kun Ismiyatin, Theresia Indah Budhy S (2022) Hydrogel Scaffold in Pulp Dentin Complex Regeneration. *J Inter Dent and Med Res* 1300
- Farag M.M (2023) Recent trends on biomaterials for tissue regeneration applications: review. *J Mater Sci* 58: 527–558
- Goldberg, M. Smith (2004) Cells and Extracellular Matrices of Dentin and pulp : A Biological Basis for repair and Tissue Engineering. *Crit. Rev. Oral Biol Med* 15(1):13-27
- Gong T, Heng BC, Lo ECM, Zhang C (2016) Current advance and future prospects of tissue engineering approach to dentin/pulp regenerative therapy. *Stem Cells Int* Article ID 9204574
- Grawish ME, LM Grawish, HM Grawish, MM Grawish, SA El-Negoly (2022) Challenges of Engineering Biomimetic Dental and Paradental Tissues. *Tissue Eng Regen Med* 17: 403–421
- Griffith LG, Naughton G (2002) Tissue engineering-current challenges and expanding opportunities. *Sci* 295(5557):1009-1014
- Gritsch L, Gioacchino Conoscentic, Vincenzo L, Carrubac, Patcharakamon Noeaidf, Aldo R. Boccaccinia (2019) Polylactide-based materials science strategies to improve tissue-material interface without the use of growth factors or other biological molecules. *Mater Sci and Eng* 94:1083-1101
- Gronthos S, Mankani M, Brahimi J, Robey PG, Shi S (2000) Postnatal human dental pulp stem cells (DPSCs) in vitro and in vivo. *Nat Aca of Sci* 97(25):13625-13630
- Hollister, Scott J, Cheng Yu Lin (2007) Computational design of tissue engineering scaffolds. *Comput Methods Appl Mech Eng* 196 (31-32):2991-2998
- Huang GT (2009) Pulp and dentin tissue engineering and regeneration: current progress. *Regen. Med* 4(5):697-707
- Hutmacher DW (2000) Scaffolds in tissue engineering bone and cartilage. *Biomater* 21(24):2529-2543

- Iranmanesh P, Ehsani A, Khademi A, Asefnejad S, Shahriari M, Soleimani (2022) Application of 3D Bioprinters for Dental Pulp Regeneration and Tissue Engineering (Porous architecture). *Transp Porous Med* 142:265-293
- Kempen DH, Lu L, Kim C, Zhu X, Dhert WJ, Currier BL, Yaszemski MJ (2006) Controlled drug release from a novel injectable biodegradable microsphere/scaffold composite based on poly (propylene fumarate). *J Biomed Mat Res* 77(1):103-111
- Langer R (2007) Tissue engineering: perspectives, challenges, and future directions. *Tissue Eng* 13(1):1
- Li L, Tang Q, Wang A, Chen Y (2019) Regrowing a tooth: in vitro and in vivo approaches. *Curr Opin. Cell Biol* 61:126-131
- Leite ML, DG Soares, G Anovazzi, IP Mendes Soares, J Hebling, CA de Souza Costa (2021) Development of fibronectin loaded nanofiber scaffolds for guided tissue regeneration. *J Biomed Mat Res* 109:1244-1258
- Linde A, Goldberg M (1993) Dentinogenesis. *Crit. Rev. Oral Biol Med* 4(5):679-728
- Liu C, Xia Z, Czernuszka J (2007) Design and development of three-dimensional scaffolds for tissue engineering. *Chem Eng Res Des* 85(7):1051-1064
- Matai I, Kaur G, Seyedsalehi A, McClinton A, Laurencin CT (2020) Progress in 3D bioprinting technology for tissue/organ regenerative engineering. *Biomaterials* 226:119536
- Noohi P, MJ Abdekhodaie, MH Nekoofar, KM Galler, PMH Dummer M (2022) Advances in scaffolds used for pulp-dentine complex tissue engineering: A narrative review. *Int Endod J* 00:1-40
- O'Brien F.J (2011) Biomaterials and scaffolds for tissue engineering. *Materials Today* 14:88-95
- Ozcan B, Bayrak E, Eriskan C (2016) Characterization of human dental pulp tissue under oscillatory shear and compression. *J Biomech Eng* (6):138
- Palma P, Ramos JC, Martins JB, Diogenes A, Figueiredo MH, Ferreira P, Viegas C, Santo JM (2017) Histologic evaluation of regenerative endodontic procedures with the use of chitosan scaffolds in immature dog teeth with apical. *J Endo* 43:1279-1287
- Pashley DH (1996) Dynamics of the pulpo-dentin complex. *Crit Rev Oral Biol Med* 7(2):104-133
- Peters OA, Paranjpe A, Gaudin A (2021) Dentine-pulp complex regeneration. *Reg App in Dentistry* 35-62
- Rabkin E, Schoen FJ (2002) Cardiovascular tissue engineering. *Cardio Path* 11(6):305-317
- Rodrigues N, M Benning, Ana M. Ferreira, L Dixon, K Dalgarno (2016) Manufacture and characterisation of porous PLA scaffold. *Procedia Cirp* 49:33-38
- Sharpe PT, Young CS (2005) Test-tube teeth. *Sci Ameri* 293(2):34-41
- Qu T, J Jing, Y Ren, C Ma, JQ Feng, Q Yu, X Liu (2015) Complete pulp-dentin complex regeneration by modulating the stiffness of biomimetic matrix. *Acta Biomat* 16:60-70
- Trope M (2010) Treatment of the immature tooth with a non-vital pulp and apical periodontitis. *Dental clinics* 54(2):313-324
- Tsou CH, Chi-Hui, Wei-Hua Yao, Yi-Cheng Lu, Chih-Yuan Tsou, Chin-San Wu, Jian Chen, Ruo Yao Wang, Chaochin Su, Wei-Song Hung, Manuel De Guzman (2017) Antibacterial property and cytotoxicity of poly(lactic acid) / nanosilver-doped multiwall carbon nanotube nanocomposite. *Polymers* 9(3):100
- Vail N, Swain L, Fox W, Aufdemorte T, Lee G, Barlow J (1999) Materials for biomedical applications. *Mat Des* 20(2-3):123-132
- Vijayavenkataraman S, Fuh JY, Lu WF (2017) 3D printing and 3D bioprinting in pediatrics. *Bio eng* 4(3):63
- Yu H, Zhang X, Song W, Pan T, Wang H, Ning T, Wei Q, Xu HH, Wu B, Ma D (2019) Effects of 3-dimensional bioprinting alginate/gelatin hydrogel scaffold extract on proliferation and differentiation of human dental pulp stem cells. *J Endod* 45(6):706-715
- Zhang L, Morsi Y, Wang Y, Li Y, Ramakrishna S (2013) Review scaffold design and stem cells for tooth regeneration. *Jpn Dent Sci Rev* 49(1):14-26